Instructive discussion of an effective block algorithm for baryon-baryon correlators

Hidekatsu Nemura

Centre for Computational Sciences, University of Tsukuba, Tsukuba, Ibaraki, 305-8577, Japan

Abstract

We describe an approach for the efficient calculation of a large number of four-point correlation functions for various baryon-baryon (BB) channels, which are the primary quantities for studying the nuclear and hyperonic nuclear forces from lattice quantum chromodynamics. Using the four-point correlation function of a proton-Λ system as a specific example, we discuss how an effective block algorithm significantly reduces the number of iterations. The effective block algorithm is applied to calculate 52 channels of the four-point correlation functions from nucleon$-$nucleon to $\Xi-\Xi$, in order to study the complete set of isospin symmetric BB interactions. The elapsed times measured for hybrid parallel computation on BlueGene/Q demonstrate that the performance of the present algorithm is reasonable for various combinations of the number of OpenMP threads and the number of MPI nodes. The numerical results are compared with the results obtained using the unified contraction algorithm for all computed sites of the 52 four-point correlators.

Keywords: nuclear force, lattice QCD, hyperon-nucleon interaction, hypernuclei

1. Introduction

Determining how the nuclear force is described from a fundamental perspective is a challenging problem in physics. Characterising an atomic nucleus as a nucleonic many body system provides successful results although

a nucleon is not a true rudimentary constituent of atomic nuclei but a composition of quarks and gluons defined in quantum chromodynamics (QCD), which is the theory of the strong interaction. For example, high-precision nucleon-nucleon (NN) potentials are available to describe the NN scattering data at low energies as well as the deuteron properties [1, 2]. The energy levels of light nuclei are well reproduced by such an NN potential together with a three-nucleon force [3, 4]. However, in contrast to the normal nuclear force, phenomenological descriptions of hyperon-nucleon (YN) and hyperon-hyperon (YY) interactions are not well constrained from experimental data because of the short life time of hyperons. The precise determination of NN, YN, and YY interactions has a large impact on the studies of both hypernuclei [5, 6, 7] and the hyperonic matter inside neutron stars [8, 9, 10, 11].

Recently, a new lattice-QCD-based method for studying the inter hadronic interactions has been proposed [12]. In this method, the interhadron potential can be obtained first from lattice QCD by measuring the Nambu-Bethe-Salpeter (NBS) wave function. The observables such as the phase shifts and the binding energies are calculated using the resultant potential [13]. This approach has been applied to various baryonic interactions [14, 15, 16, 17, 18, 19, 20, 21, 22, 23, 24, 25], and has been recently extended to systems in inelastic channels [26, 27, 28]. This approach is now called HAL QCD method because almost all the recent developments cited above have been provided by the HAL QCD Collaboration. The flavour symmetry breaking is a key topic in the study of the isospin symmetric baryon-baryon (BB) interactions based on the $2 + 1$ flavour lattice QCD. In such a situation, it is advantageous to calculate a large number of NBS wave functions of various BB channels simultaneously in a single lattice QCD calculation. Therefore, an efficient approach for performing such a computationally demanding lattice QCD calculation is crucial.

The purpose of this paper is to describe a practicable algorithm that can efficiently compute a large number of four-point correlation functions of various BB systems. The contraction algorithm considered in this paper is different from the unified contraction algorithm [29] and has been used to calculate the ΛN and ΣN potentials [30, 31, 32]. This is a reasonable approach for computing the various BB correlators efficaciously. Methods following different approach for large baryon number systems are found in Refs. [33, 34]. The paper is organised as follows: Section 2 outlines a basic formulation of the HAL QCD approach. Section 3 describes an approach for calculating the four-point correlation function by considering the $p\Lambda$ system

2

as an example. The present contraction algorithm is generalised to various BB systems in Section 4. In Sec. 5 we demonstrate the hybrid parallel computation of the four-point correlation functions. The numerical results calculated by the hybrid parallel program are compared with the results from the unified contraction algorithm in Sec. 6. Sec. 7 summarises the paper.

2. Outline of the HAL QCD method

In the study of the nuclear force using the HAL QCD approach, the equal time NBS wave function with Euclidean time t is a vital quantity, which is defined by[12, 13]

$$\phi_E(\vec{r})e^{-Et} = \sum_{\vec{X}} \left\langle 0 \left| B_{1,\alpha}(\vec{X} + \vec{r}, t) B_{2,\beta}(\vec{X}, t) \right| B = 2, E \right\rangle, \quad (1)$$

where $E = \sqrt{k^2 + m_{B_1}^2} + \sqrt{k^2 + m_{B_2}^2}$ is the total energy in the centre of mass system of a baryon number $B = 2$ state with masses m_{B_1} and m_{B_2}. $B_{1,\alpha}(x)$ $(B_{2,\beta}(x))$ denotes the local interpolating field of baryon B_1 (B_2). For simplicity, we consider a two-nucleon system in the isospin symmetric limit. Thus, $m_{B_1} = m_{B_2} = m_N$ and the $B_{1,\alpha} = p_\alpha$ $(B_{2,\beta} = n_\beta)$ is the local interpolating field of proton (neutron) given by

$$p_\alpha(x) = \varepsilon_{abc} \left(u_a(x) C \gamma_5 d_b(x) \right) u_{c\alpha}(x), \quad n_\beta(y) = -\varepsilon_{abc} \left(u_a(y) C \gamma_5 d_b(y) \right) d_{c\beta}(y), \quad (2)$$

where $u_{c\alpha}(x)$ $(d_{c\beta}(x))$ is the up (down) quark field with the colour indices denoted by a, b, and c, and the Dirac spinors denoted by α and β. The ε_{abc} is the totally anti-symmetric tensor and $C = \gamma_4 \gamma_2$ is the charge conjugation matrix. For simplicity, we have suppressed the dummy spinor indices in the round brackets. Based on the NBS wave function, we define a non-local but energy-independent potential $\left(\frac{\nabla^2}{2\mu} - \frac{k^2}{2\mu} \right) \phi_E(\vec{r}) = \int d^3 r' U(\vec{r}, \vec{r'}) \phi_E(\vec{r'})$ with the reduced mass $\mu = m_N/2$. An important point of the HAL QCD method is that the potential defined above gives the correct scattering phase shift of the S-matrix for all values of k in the elastic region, $E < E_{\text{th}} \equiv 2m_N + m_\pi$, with the pion mass m_π, by construction. A more detailed account of the relation between the NBS wave function and the S-matrix in QCD is found in the appendix A of Ref. [13].

In lattice QCD calculations, we compute the normalised four-point correlation function defined by[20]

$$R_{\alpha\beta}^{(J,M)}(\vec{r}, t - t_0)$$
$$= \sum_{\vec{X}} \left\langle 0 \middle| B_{1,\alpha}(\vec{X}+\vec{r}, t) B_{2,\beta}(\vec{X}, t) \overline{\mathcal{J}_{B_3 B_4}^{(J,M)}(t_0)} \middle| 0 \right\rangle / \exp\{-(m_{B_1}+m_{B_2})(t-t_0)\}, \quad (3)$$

where $\overline{\mathcal{J}_{B_3 B_4}^{(J,M)}(t_0)} = \sum_{\alpha'\beta'} P_{\alpha'\beta'}^{(J,M)} \overline{B_{3,\alpha'}(t_0) B_{4,\beta'}(t_0)}$ is a source operator that creates $B_3 B_4$ ($=pn$) states with the total angular momentum J, M. The normalised four-point function can be expressed as

$$R_{\alpha\beta}^{(J,M)}(\vec{r}, t - t_0)$$
$$= \sum_n A_n \sum_{\vec{X}} \left\langle 0 \middle| B_{1,\alpha}(\vec{X}+\vec{r}, 0) B_{2,\beta}(\vec{X}, 0) \middle| E_n \right\rangle e^{-(E_n - m_{B_1} - m_{B_2})(t-t_0)}$$
$$+ O(e^{-(E_{\rm th} - m_{B_1} - m_{B_2})(t-t_0)}), \quad (4)$$

where E_n ($|E_n\rangle$) is the eigen-energy (eigen-state) of the six-quark system and $A_n = \sum_{\alpha'\beta'} P_{\alpha'\beta'}^{(JM)} \langle E_n | \overline{B}_{4,\beta'} \overline{B}_{3,\alpha'} | 0 \rangle$. At moderately large $t - t_0$ where the inelastic contribution above the pion production $O(e^{-(E_{\rm th} - 2m_N)(t-t_0)}) = O(e^{-m_\pi(t-t_0)})$ becomes exiguous, we can construct the non-local potential U through $\left(\frac{\nabla^2}{2\mu} - \frac{k^2}{2\mu}\right) R(\vec{r}) = \int d^3 r' U(\vec{r}, \vec{r'}) R(\vec{r'})$. In lattice QCD calculations in a finite box, it is practical to use the velocity (derivative) expansion, $U(\vec{r}, \vec{r'}) = V(\vec{r}, \vec{\nabla}_r) \delta^3(\vec{r} - \vec{r'})$. In the lowest few orders we have

$$V(\vec{r}, \vec{\nabla}_r) = \underbrace{V_0(r) + V_\sigma(r)\vec{\sigma}_1 \cdot \vec{\sigma}_2 + V_T(r) S_{12}}_{V_{LO}} + \underbrace{V_{LS}(r)\vec{L} \cdot (\vec{\sigma}_1 + \vec{\sigma}_2)}_{V_{NLO}} + O(\nabla^2),$$

(5)

where $r = |\vec{r}|$, $\vec{\sigma}_i$ are the Pauli matrices acting on the spin space of the i-th baryon, $S_{12} = 3(\vec{r} \cdot \vec{\sigma}_1)(\vec{r} \cdot \vec{\sigma}_2)/r^2 - \vec{\sigma}_1 \cdot \vec{\sigma}_2$ is the tensor operator, and $\vec{L} = \vec{r} \times (-i\vec{\nabla})$ is the angular momentum operator. The first three-terms constitute the leading order (LO) potential while the fourth term corresponds to the next-to-leading order (NLO) potential. By taking the non-relativistic approximation, $E_n - m_{B_1} - m_{B_2} \simeq k_n^2/(2\mu) + O(k_n^4)$, and neglecting the $V_{\rm NLO}$ and the higher order terms, we obtain $\left(\frac{\nabla^2}{2\mu} - \frac{\partial}{\partial t}\right) R(\vec{r}, t) \simeq V_{\rm LO}(\vec{r}) R(\vec{r}, t)$. For the spin singlet state, we extract the central potential as $V_C(r; J = 0) =$

$(\frac{\nabla^2}{2\mu} - \frac{\partial}{\partial t})R/R$. For the spin triplet state, the wave function is decomposed into the S- and D-wave components as

$$\begin{cases} R_{\alpha\beta}(\vec{r};\ ^3S_1) = \mathcal{P}R_{\alpha\beta}(\vec{r}; J=1) \equiv \frac{1}{24}\sum_{\mathcal{R}\in O}\mathcal{R}R_{\alpha\beta}(\vec{r}; J=1), \\ R_{\alpha\beta}(\vec{r};\ ^3D_1) = \mathcal{Q}R_{\alpha\beta}(\vec{r}; J=1) \equiv (1-\mathcal{P})R_{\alpha\beta}(\vec{r}; J=1). \end{cases} \tag{6}$$

Therefore, the Schrödinger equation with the LO potentials for the spin triplet state becomes

$$\left\{ \begin{matrix} \mathcal{P} \\ \mathcal{Q} \end{matrix} \right\} \times \left\{ -\frac{\nabla^2}{2\mu} + V_0(r) + V_\sigma(r)(\vec{\sigma}_1 \cdot \vec{\sigma}_2) + V_T(r)S_{12} \right\} R(\vec{r}, t-t_0)$$
$$= -\left\{ \begin{matrix} \mathcal{P} \\ \mathcal{Q} \end{matrix} \right\} \times \frac{\partial}{\partial t}\, R(\vec{r}, t-t_0), \tag{7}$$

from which the central and tensor potentials, $V_C(r; J=0) = V_0(r) - 3V_\sigma(r)$ for $J=0$, $V_C(r; J=1) = V_0(r) + V_\sigma(r)$, and $V_T(r)$ for $J=1$, can be determined[1].

The HAL QCD method mentioned above can be applied to the baryon number $B=2$ systems, including strangeness for the YN and YY potentials. In addition to the up and down quarks, we use the strange quark operator $s_{c\alpha}(x)$ to define the interpolating operators of hyperons as

$$\Sigma_\alpha^+(x) = -\varepsilon_{abc}\left(u_a(x)C\gamma_5 s_b(x)\right)u_{c\alpha}(x),\ \ \Sigma_{\bar{\beta}}^-(y) = -\varepsilon_{abc}\left(d_a(y)C\gamma_5 s_b(y)\right)d_{c\beta}(y),$$
$$\Sigma_\alpha^0(x) = \frac{1}{\sqrt{2}}\left(X_{u,\alpha}(x) - X_{d,\alpha}(x)\right),\ \ \Lambda_\beta(y) = \frac{1}{\sqrt{6}}\left(X_{u,\beta}(y) + X_{d,\beta}(y) - 2X_{s,\beta}(y)\right),$$
$$\Xi_\alpha^0(x) = \varepsilon_{abc}\left(u_a(x)C\gamma_5 s_b(x)\right)s_{c\alpha}(x),\ \ \Xi_{\bar{\beta}}^-(y) = -\varepsilon_{abc}\left(d_a(y)C\gamma_5 s_b(y)\right)s_{c\beta}(y),$$
$$\tag{8}$$

where

$$X_{u,\alpha}(x) = \varepsilon_{abc}\left(d_a(x)C\gamma_5 s_b(x)\right)u_{c\alpha}(x),\ \ X_{d,\alpha}(x) = \varepsilon_{abc}\left(s_a(x)C\gamma_5 u_b(x)\right)d_{c\alpha}(x),$$
$$X_{s,\alpha}(x) = \varepsilon_{abc}\left(u_a(x)C\gamma_5 d_b(x)\right)s_{c\alpha}(x). \tag{9}$$

---

[1] The potential is obtained from the NBS wave function at moderately large imaginary time; it would be $t - t_0 \gg 1/m_\pi \sim 1.4$ fm even for the physical pion mass. Furthermore, no single state saturation between the ground state and the first excited states, $t - t_0 \gg (\Delta E)^{-1} = \left((2\pi)^2/(2\mu L^2)\right)^{-1}$, is required for the present HAL QCD method[20], which becomes $\left((2\pi)^2/(2\mu L^2)\right)^{-1} \simeq 4.6$ fm if we consider $L \sim 6$ fm and $m_N \simeq 1$ GeV. In Ref. [14], the validity of the velocity expansion of the NN potential has been examined in quenched lattice QCD simulations at $m_\pi \simeq 530$ MeV and $L \simeq 4.4$ fm.

In the flavour $SU(3)$ limit, the extension of the HAL QCD method to the YN and YY systems is straightforward [16, 17, 19]. For the $N_f = 2+1$ flavour lattice QCD calculations, the YN and YY potentials can be obtained in a similar fashion, where the mass difference between m_{B_1} and m_{B_2} is appropriately considered [15, 30, 31, 32]. In addition, the HAL QCD method is extended to obtain the coupled-channel potentials above the inelastic thresholds[26, 27, 28].

3. The effective block algorithm

Let us consider the four-point correlation function of a $p\Lambda$ system as a specific example. In what follows, we introduce a highly abbreviated notation to indicate explicitly the colour, spinor, and spatial subscripts. For example, we express the interpolating field of proton as

$$
\begin{aligned}
p_\alpha(x) &= \varepsilon(c_1, c_2, c_3)(C\gamma_5)(\alpha_1, \alpha_2)\delta(\alpha, \alpha_3)u(\xi_1)d(\xi_2)u(\xi_3), \qquad (\xi_i = x_i\alpha_i c_i) \\
&= \varepsilon(1, 2, 3)(C\gamma_5)(1, 2)\delta(\alpha, 3)u(1)d(2)u(3).
\end{aligned}
$$
(10)

Here, in the last equation, the numbers in the round brackets show the indices of colour for $\varepsilon(\cdot)$, the indices of Dirac spinor for $(C\gamma_5)(\cdot)$ and $\delta(\cdot)$ and the indices both of colour, spinor, and spatial coordinate for the quark fields $u(\cdot)$, $d(\cdot)$, and $s(\cdot)$ [2]. By using the abbreviated notations, the $p\Lambda$ four-point correlator is given by

$$
\begin{aligned}
&R_{\alpha\beta\alpha'\beta'}(\vec{r}, t - t_0) \\
&= \sum_{\vec{X}} \left\langle 0 \left| p_\alpha(\vec{X} + \vec{r}, t)\Lambda_\beta(\vec{X}, t)\overline{\mathcal{J}_{p_{\alpha'}\Lambda_{\beta'}}(t_0)} \right| 0 \right\rangle / \exp\{-(m_p + m_\Lambda)(t - t_0)\}
\end{aligned}
$$

---

[2] In this paper, we take a conventional choice of the baryon's interpolating field given in Eqs. (2), (8)−(9) which is expected to have large overlap with the single baryon's ground state. Utilising more general form of the baryon's interpolating field is straightforward. We may replace, for example, the baryon's interpolating field as

$$
B_\gamma = \varepsilon_{abc}\left((q_{1,a}\Gamma_1 q_{2,b})\Gamma_2 q_{3,c}\right),
$$
(11)

where q_1, q_2, and q_3 denote particular quark flavours to form baryon B and the set of gamma matrices $\{\Gamma_1, \Gamma_2\}$ is appropriately taken so as to carry the quantum numbers of baryon B with combined spinor-space-time subscript γ. Even for the general case, we can follow the procedure in this section with taking two replacements everywhere: (i) $(C\gamma_5)(\alpha, \alpha') \to \Gamma_1(\alpha, \alpha')$ and (ii) $\delta(\alpha, \alpha') \to \Gamma_2(\alpha, \alpha')$.

$$= \sum_{\vec{X}} \frac{1}{6} \mathrm{e}^{(m_p + m_\Lambda)(t - t_0)} \varepsilon(1, 4, 2) \varepsilon(5, 6, 3) \varepsilon(1', 4', 2') \varepsilon(5', 6', 3')$$

$$\times (C\gamma_5)(1, 4) \delta(\alpha, 2)(C\gamma_5)(1', 4') \delta(\alpha', 2')$$
$$\times \{(C\gamma_5)(5, 6) \delta(\beta, 3) + (C\gamma_5)(6, 3) \delta(\beta, 5) - 2(C\gamma_5)(3, 5) \delta(\beta, 6)\}$$
$$\times \{(C\gamma_5)(5', 6') \delta(\beta', 3') + (C\gamma_5)(6', 3') \delta(\beta', 5') - 2(C\gamma_5)(3', 5') \delta(\beta', 6')\}$$
$$\times \langle u(1) d(4) u(2) d(5) s(6) u(3) \bar{u}(3') \bar{s}(6') \bar{d}(5') \bar{u}(2') \bar{d}(4') \bar{u}(1') \rangle, \qquad (12)$$

where
$$\vec{x}_1 = \vec{x}_2 = \vec{x}_4 = \vec{X} + \vec{r}, \qquad \vec{x}_3 = \vec{x}_5 = \vec{x}_6 = \vec{X}. \qquad (13)$$

The last line in Eq. (12) is evaluated through the Wick's contraction and represented in terms of quark propagators $\langle q(\xi_i) \bar{q}(\xi'_j) \rangle = \langle q(i) \bar{q}(j') \rangle$,

$$\langle u(1) d(4) u(2) d(5) s(6) u(3) \bar{u}(3') \bar{s}(6') \bar{d}(5') \bar{u}(2') \bar{d}(4') \bar{u}(1') \rangle$$

$$= \left(\langle u(3)\bar{u}(3') \rangle \det \begin{vmatrix} \langle u(1)\bar{u}(1') \rangle & \langle u(1)\bar{u}(2') \rangle \\ \langle u(2)\bar{u}(1') \rangle & \langle u(2)\bar{u}(2') \rangle \end{vmatrix} \langle d(4)\bar{d}(4') \rangle \langle d(5)\bar{d}(5') \rangle \right.$$

$$- \langle u(3)\bar{u}(2') \rangle \det \begin{vmatrix} \langle u(1)\bar{u}(1') \rangle & \langle u(1)\bar{u}(3') \rangle \\ \langle u(2)\bar{u}(1') \rangle & \langle u(2)\bar{u}(3') \rangle \end{vmatrix} \langle d(4)\bar{d}(4') \rangle \langle d(5)\bar{d}(5') \rangle$$

$$- \langle u(3)\bar{u}(3') \rangle \det \begin{vmatrix} \langle u(1)\bar{u}(1') \rangle & \langle u(1)\bar{u}(2') \rangle \\ \langle u(2)\bar{u}(1') \rangle & \langle u(2)\bar{u}(2') \rangle \end{vmatrix} \langle d(4)\bar{d}(5') \rangle \langle d(5)\bar{d}(4') \rangle$$

$$+ \langle u(3)\bar{u}(2') \rangle \det \begin{vmatrix} \langle u(1)\bar{u}(1') \rangle & \langle u(1)\bar{u}(3') \rangle \\ \langle u(2)\bar{u}(1') \rangle & \langle u(2)\bar{u}(3') \rangle \end{vmatrix} \langle d(4)\bar{d}(5') \rangle \langle d(5)\bar{d}(4') \rangle$$

$$+ \langle u(3)\bar{u}(1') \rangle \det \begin{vmatrix} \langle u(1)\bar{u}(2') \rangle & \langle u(1)\bar{u}(3') \rangle \\ \langle u(2)\bar{u}(2') \rangle & \langle u(2)\bar{u}(3') \rangle \end{vmatrix} \langle d(4)\bar{d}(4') \rangle \langle d(5)\bar{d}(5') \rangle$$

$$\left. - \langle u(3)\bar{u}(1') \rangle \det \begin{vmatrix} \langle u(1)\bar{u}(2') \rangle & \langle u(1)\bar{u}(3') \rangle \\ \langle u(2)\bar{u}(2') \rangle & \langle u(2)\bar{u}(3') \rangle \end{vmatrix} \langle d(4)\bar{d}(5') \rangle \langle d(5)\bar{d}(4') \rangle \right)$$

$$\times \langle s(6)\bar{s}(6') \rangle. \qquad (14)$$

The six terms in Eq. (14) can be depicted with six diagrams as shown in Fig. 1.

The Eq. (12) includes implicit summations such as $\sum_{c_1, \cdots, c_6} \sum_{\alpha_1, \cdots, \alpha_6} \sum_{c'_1, \cdots, c'_6} \sum_{\alpha'_1, \cdots, \alpha'_6}$; the number of iterations for each summation is $N_c = 3$ for the colour or $N_\alpha = 4$ for the Dirac spinor. Combining the iteration due to the Wick contraction, for the system with the baryon number B in general, the total number of iterations for such a correlator is in a naive counting $(N_c! N_\alpha)^{2B} \times N_u! N_d! N_s!$, where the N_u, N_d, and N_s are the numbers of u-quark, d-quark, and s-quark, respectively; thus the numbers satisfy
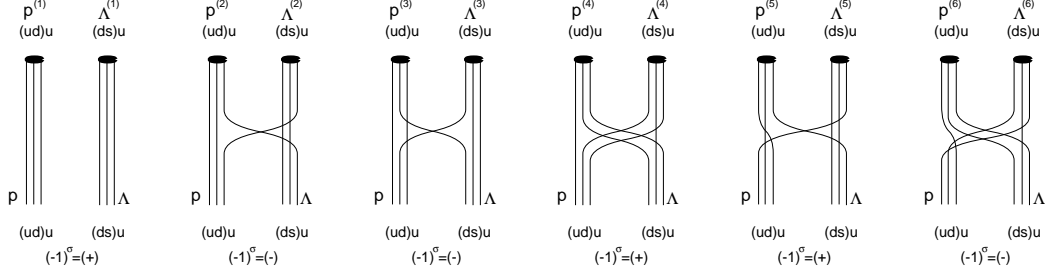
Figure 1: Diagrammatic representation of the four-point correlation function $\langle p\Lambda \overline{p\Lambda}\rangle$. The six diagrams correspond to the six terms of Eq. (14). The cyclic permutations for the quark fields $(ds)u \to (su)d \to (ud)s$ are taken into account in the interpolating field of Λ, which correspond to the contributions from the X_u, X_d, and X_s. The parity of each permutation is also shown as $(-1)^\sigma$.

$N_u + N_d + N_s = 3B$. Clearly, the above counting is too naive though curtailment of the number of iterations is not trivial. We now explain briefly how the number of iterations reduces when we calculate the four-point correlation function of the $p\Lambda$ system [30]. In Ref. [15], only the limited spatial points were evaluated on a L^3 lattice because of the computational cost $O(L^6)$ in the primitive numerical approach. In this paper we employ the Fast-Fourier-Transform (FFT) to improve the numerical performance to $O(L^3 \log L^3)$; we consider the diagrammatic classification of the Wick contraction in order to make better use of the FFT.

$$
\begin{aligned}
R_{\alpha\beta\alpha'\beta'}(\vec{r}) &= \sum_{i=1}^{6} F_i \sum_{\vec{X}} \left([p_\alpha^{(i)}](\vec{X}+\vec{r}) \times [\Lambda_\beta^{(i)}](\vec{X}) \right)_{\alpha'\beta'} \\
&= \frac{1}{L^3} \sum_{\vec{q}} \left(\sum_{i=1}^{6} F_i \left(\widetilde{[p_\alpha^{(i)}]}(\vec{q}) \times \widetilde{[\Lambda_\beta^{(i)}]}(-\vec{q}) \right)_{\alpha'\beta'} \right) e^{i\vec{q}\cdot\vec{r}}, \quad (15)
\end{aligned}
$$

where $\widetilde{[p_\alpha^{(i)}]}(\vec{q}) = \sum_{\vec{x}}[p_\alpha^{(i)}](\vec{x})e^{-i\vec{q}\cdot\vec{x}}$, $\widetilde{[\Lambda_\beta^{(i)}]}(\vec{q}) = \sum_{\vec{x}}[\Lambda_\beta^{(i)}](\vec{x})e^{-i\vec{q}\cdot\vec{x}}$, and $F_i = (-1)^{\sigma_i}(1/6)e^{(m_p+m_\Lambda)(t-t_0)}$ with $\sigma_i = $ even(odd) for the even (odd) permutations. We omit the explicit $(t-t_0)$ dependence both of $R_{\alpha\beta\alpha'\beta'}$, $[p_\alpha^{(i)}]$, and $[\Lambda_\beta^{(i)}]$. Six diagrams in Fig. 1 correspond to the six baryon-block pairs $([p_\alpha^{(1)}] \times [\Lambda_\beta^{(1)}]), \cdots, ([p_\alpha^{(6)}] \times [\Lambda_\beta^{(6)}])$. Note that the number of diagrams is reduced by the factor $2^{B-N_\Lambda-N_{\Sigma^0}}$ since the exchange between identical quarks in each baryon operator in the sink shall be taken into account in the construction of each baryon block $[p_\alpha^{(i)}]$ or $[\Lambda_\beta^{(i)}]$, where $N_\Lambda(N_{\Sigma^0})$ is the number

of Λ (Σ^0) in the sink. We present the explicit forms of the baryon blocks. For simplicity, we consider only the contributions from $\overline{X}_u$ in the $\overline{\Lambda}_{\beta'}$ in the source for a while and omit the contributions from the $\overline{X}_d$ and $\overline{X}_s$ operators. The contributions from $\overline{X}_d$ and $\overline{X}_s$ are discussed later.

(i) $\boldsymbol{p_\alpha^{(1)}}$ and $\boldsymbol{\Lambda_\beta^{(1)}}$

The first diagram is the simplest case:

$$R_{\alpha\beta\alpha'\beta'}^{(1)}(\vec{r}) = \sum_{\vec{X}} \left([p_\alpha^{(1)}](\vec{X}+\vec{r}) \times [\Lambda_\beta^{(1)}](\vec{X}) \right)_{\alpha'\beta'} = \sum_{\vec{X}} [p_{\alpha\alpha'}^{(1)}](\vec{X}+\vec{r})[\Lambda_{\beta\beta'}^{(1)}](\vec{X}),$$
(16)

where

$$
\begin{aligned}
& [p_{\alpha\alpha'}^{(1)}](\vec{x}) \\
= & \ \varepsilon(1,4,2)(C\gamma_5)(1,4)\delta(\alpha,2)\varepsilon(1',4',2')(C\gamma_5)(1',4')\delta(\alpha',2') \\
& \times \det \left| \begin{matrix} \langle u(1)\bar{u}(1') \rangle & \langle u(1)\bar{u}(2') \rangle \\ \langle u(2)\bar{u}(1') \rangle & \langle u(2)\bar{u}(2') \rangle \end{matrix} \right| \langle d(4)\bar{d}(4') \rangle,
\end{aligned}
$$
(17)

$$
\begin{aligned}
& [\Lambda_{\beta\beta'}^{(1)}](\vec{y}) \\
= & \ \varepsilon(5,6,3) \left\{ (C\gamma_5)(5,6)\delta(\beta,3) + (C\gamma_5)(6,3)\delta(\beta,5) - 2(C\gamma_5)(3,5)\delta(\beta,6) \right\} \\
& \times \varepsilon(5',6',3')(C\gamma_5)(5',6')\delta(\beta',3')\langle u(3)\bar{u}(3') \rangle\langle d(5)\bar{d}(5') \rangle\langle s(6)\bar{s}(6') \rangle.
\end{aligned}
$$
(18)

This is just a product of two two-point correlation functions. The summations of all internal indices can be performed prior to evaluating the FFT. This fact significantly slashes in the computational cost; the reduction factor at the first diagram is $(N_c! N_\alpha)^2 \times 2^{B-N_\Lambda-N_{\Sigma^0}}/1 = 1152$.

(ii) $\boldsymbol{p_\alpha^{(2)}}$ and $\boldsymbol{\Lambda_\beta^{(2)}}$

The second diagram shows an one-quark exchange in u quarks:

$$
\begin{aligned}
R_{\alpha\beta\alpha'\beta'}^{(2)}(\vec{r}) &= \sum_{\vec{X}} \left([p_\alpha^{(2)}](\vec{X}+\vec{r}) \times [\Lambda_\beta^{(2)}](\vec{X}) \right)_{\alpha'\beta'} \\
&= \sum_{\vec{X}} \sum_{c_2', c_3'} [p_{\alpha\beta'}^{(2)}](\vec{X}+\vec{r}; c_2', c_3')[\Lambda_{\beta\alpha'}^{(2)}](\vec{X}; c_2', c_3'),
\end{aligned}
$$
(19)

where

$$
\begin{aligned}
& [p_{\alpha\beta'}^{(2)}](\vec{x}; c_2', c_3') \\
= & \ \varepsilon(1,4,2)(C\gamma_5)(1,4)\delta(\alpha,2)\varepsilon(1',4',2')(C\gamma_5)(1',4')\delta(\beta',3')
\end{aligned}
$$

9

$$\times \det \begin{vmatrix} \langle u(1)\bar{u}(1') \rangle & \langle u(1)\bar{u}(3') \rangle \\ \langle u(2)\bar{u}(1') \rangle & \langle u(2)\bar{u}(3') \rangle \end{vmatrix} \langle d(4)\bar{d}(4') \rangle, \tag{20}$$

$$
\begin{aligned}
& [\Lambda^{(2)}_{\beta\alpha'}](\vec{y}; c'_2, c'_3) \\
={} & \varepsilon(5,6,3)\{(C\gamma_5)(5,6)\delta(\beta,3) + (C\gamma_5)(6,3)\delta(\beta,5) - 2(C\gamma_5)(3,5)\delta(\beta,6)\} \\
& \times \varepsilon(5',6',3')(C\gamma_5)(5',6')\delta(\alpha',2')\langle u(3)\bar{u}(2') \rangle \langle d(5)\bar{d}(5') \rangle \langle s(6)\bar{s}(6') \rangle. \tag{21}
\end{aligned}
$$

We have additional arguments, (c'_2, c'_3), for the baryon blocks $[p^{(2)}_\alpha]$ and $[\Lambda^{(2)}_\beta]$ because of the exchange of the quark fields in the source. Note that the $\delta(\alpha', 2')$ in $\bar{p}_{\alpha'}$ and the $\delta(\beta', 3')$ in $\bar{\Lambda}_{\beta'}$ are also exchanged between the baryon blocks $[p^{(2)}_{\alpha\beta'}]$ and $[\Lambda^{(2)}_{\beta\alpha'}]$ so that the two outer indices in the source $(\alpha'\beta')$ are crossed as $[p^{(2)}_{\alpha\beta'}]$ and $[\Lambda^{(2)}_{\beta\alpha'}]$. Performed these manipulations, the number of explicit summations of indices reduces to only two colours which makes the reduction factor $(N_c! N_\alpha)^2 \times 2^{B-N_\Lambda-N_{\Sigma^0}}/(N_c^2) = 128$.

(iii) $\boldsymbol{p^{(3)}_\alpha}$ and $\boldsymbol{\Lambda^{(3)}_\beta}$
    This case has an exchange in d quarks:

$$
\begin{aligned}
R^{(3)}_{\alpha\beta\alpha'\beta'}(\vec{r}) &= \sum_{\vec{X}} \left([p^{(3)}_\alpha](\vec{X}+\vec{r}) \times [\Lambda^{(3)}_\beta](\vec{X}) \right)_{\alpha'\beta'} \\
&= \sum_{\vec{X}} \sum_{c'_4, c'_5, \alpha'_4, \alpha'_5} [p^{(3)}_{\alpha\alpha'}](\vec{X}+\vec{r}; c'_4, c'_5, \alpha'_4, \alpha'_5)[\Lambda^{(3)}_{\beta\beta'}](\vec{X}; c'_4, c'_5, \alpha'_4, \alpha'_5), \tag{22}
\end{aligned}
$$

where

$$
\begin{aligned}
& [p^{(3)}_{\alpha\alpha'}](\vec{x}; c'_4, c'_5, \alpha'_4, \alpha'_5) \\
={} & \varepsilon(1,4,2)(C\gamma_5)(1,4)\delta(\alpha,2)\varepsilon(1',4',2')(C\gamma_5)(1',4')\delta(\alpha',2') \\
& \times \det \begin{vmatrix} \langle u(1)\bar{u}(1') \rangle & \langle u(1)\bar{u}(2') \rangle \\ \langle u(2)\bar{u}(1') \rangle & \langle u(2)\bar{u}(2') \rangle \end{vmatrix} \langle d(4)\bar{d}(5') \rangle, \tag{23}
\end{aligned}
$$

$$
\begin{aligned}
& [\Lambda^{(3)}_{\beta\beta'}](\vec{y}; c'_4, c'_5, \alpha'_4, \alpha'_5) \\
={} & \varepsilon(5,6,3)\{(C\gamma_5)(5,6)\delta(\beta,3) + (C\gamma_5)(6,3)\delta(\beta,5) - 2(C\gamma_5)(3,5)\delta(\beta,6)\} \\
& \times \varepsilon(5',6',3')(C\gamma_5)(5',6')\delta(\beta',3')\langle u(3)\bar{u}(3') \rangle \langle d(5)\bar{d}(4') \rangle \langle s(6)\bar{s}(6') \rangle. \tag{24}
\end{aligned}
$$

The number of explicit summations of indices reduces to two colours and two spinors, which makes the reduction factor $(N_c! N_\alpha)^2 \times 2^{B-N_\Lambda-N_{\Sigma^0}}/(N_c^2 N_\alpha^2) = 8$.

(iv) $\boldsymbol{p^{(4)}_\alpha}$ and $\boldsymbol{\Lambda^{(4)}_\beta}$

This is one of two-quark exchange diagrams in the $\langle p\Lambda \overline{p\Lambda}\rangle$:

$$R^{(4)}_{\alpha\beta\alpha'\beta'}(\vec{r}) = \sum_{\vec{X}} \left([p^{(4)}_\alpha](\vec{X}+\vec{r}) \times [\Lambda^{(4)}_\beta](\vec{X}) \right)_{\alpha'\beta'}$$

$$= \sum_{\vec{X}} \sum_{c'_1,c'_6,\alpha'_1,\alpha'_6} [p^{(4)}_{\alpha\beta'}](\vec{X}+\vec{r}; c'_1,c'_6,\alpha'_1,\alpha'_6)[\Lambda^{(4)}_{\beta\alpha'}](\vec{X}; c'_1,c'_6,\alpha'_1,\alpha'_6) \quad (25)$$

where

$$[p^{(4)}_{\alpha\beta'}](\vec{x}; c'_1,c'_6,\alpha'_1,\alpha'_6)$$
$$= \varepsilon(1,4,2)(C\gamma_5)(1,4)\delta(\alpha,2)\varepsilon(5',6',3')(C\gamma_5)(5',6')\delta(\beta',3')$$
$$\times \det \left| \begin{array}{cc} \langle u(1)\bar{u}(1')\rangle & \langle u(1)\bar{u}(3')\rangle \\ \langle u(2)\bar{u}(1')\rangle & \langle u(2)\bar{u}(3')\rangle \end{array} \right| \langle d(4)\bar{d}(5')\rangle, \quad (26)$$

$$[\Lambda^{(4)}_{\beta\alpha'}](\vec{y}; c'_1,c'_6,\alpha'_1,\alpha'_6)$$
$$= \varepsilon(5,6,3) \left\{ (C\gamma_5)(5,6)\delta(\beta,3) + (C\gamma_5)(6,3)\delta(\beta,5) - 2(C\gamma_5)(3,5)\delta(\beta,6) \right\}$$
$$\times \varepsilon(1',4',2')(C\gamma_5)(1',4')\delta(\alpha',2')\langle u(3)\bar{u}(2')\rangle\langle d(5)\bar{d}(4')\rangle\langle s(6)\bar{s}(6')\rangle. \quad (27)$$

Note that two tensorial factors $\varepsilon(5',6',3')(C\gamma_5)(5',6')\delta(\beta',3')$ and $\varepsilon(1',4',2')(C\gamma_5)(1',4')\delta(\alpha',2')$ are exchanged between $[p^{(4)}_{\alpha\beta'}]$ and $[\Lambda^{(4)}_{\beta\alpha'}]$ due to the two-quark exchange so that the two outer source indices (α',β') are exchanged, too. The number of explicit summations of indices reduces to two colours and two spinors, which makes the reduction factor $(N_c!N_\alpha)^2 \times 2^{B-N_\Lambda-N_{\Sigma^0}}/(N_c^2 N_\alpha^2) = 8$.

(v) $p^{(5)}_\alpha$ and $\Lambda^{(5)}_\beta$

In this case we have another exchange diagram in u quarks:

$$R^{(5)}_{\alpha\beta\alpha'\beta'}(\vec{r}) = \sum_{\vec{X}} \left([p^{(5)}_\alpha](\vec{X}+\vec{r}) \times [\Lambda^{(5)}_\beta](\vec{X}) \right)_{\alpha'\beta'}$$

$$= \sum_{\vec{X}} \sum_{c'_1,c'_3,\alpha'_1} [p^{(5)}_{\alpha\alpha'\beta'}](\vec{X}+\vec{r}; c'_1,c'_3,\alpha'_1)[\Lambda^{(5)}_\beta](\vec{X}; c'_1,c'_3,\alpha'_1), \quad (28)$$

where

$$[p^{(5)}_{\alpha\alpha'\beta'}](\vec{x}; c'_1,c'_3,\alpha'_1)$$
$$= \varepsilon(1,4,2)(C\gamma_5)(1,4)\delta(\alpha,2)\varepsilon(1',4',2')(C\gamma_5)(1',4')\delta(\alpha',2')\delta(\beta',3')$$
$$\times \det \left| \begin{array}{cc} \langle u(1)\bar{u}(2')\rangle & \langle u(1)\bar{u}(3')\rangle \\ \langle u(2)\bar{u}(2')\rangle & \langle u(2)\bar{u}(3')\rangle \end{array} \right| \langle d(4)\bar{d}(4')\rangle, \quad (29)$$

11

$$[\Lambda_\beta^{(5)}](\vec{y}; c_1', c_3', \alpha_1')$$
$$= \varepsilon(5,6,3)\left\{(C\gamma_5)(5,6)\delta(\beta,3) + (C\gamma_5)(6,3)\delta(\beta,5) - 2(C\gamma_5)(3,5)\delta(\beta,6)\right\}$$
$$\times \varepsilon(5',6',3')(C\gamma_5)(5',6')\langle u(3)\bar{u}(1')\rangle\langle d(5)\bar{d}(5')\rangle\langle s(6)\bar{s}(6')\rangle. \tag{30}$$

Note that both the $\delta(\beta',3')$ in $\overline{\Lambda}_{\beta'}$ and the $\delta(\alpha',2')$ in $\overline{p}_{\alpha'}$ transfer to the baryon block $[p_{\alpha\alpha'\beta'}^{(5)}]$ so that the two outer indices in the source $(\alpha'\beta')$ are accompanied in the $[p_{\alpha\alpha'\beta'}^{(5)}]$. The number of explicit summations of indices reduces to two colours and one spinor, which makes the reduction factor $(N_c! N_\alpha)^2 \times 2^{B-N_\Lambda - N_{\Sigma^0}}/(N_c^2 N_\alpha) = 32$.

(vi) $p_\alpha^{(6)}$ and $\Lambda_\beta^{(6)}$

In this case we have another two-quark exchange diagram:

$$R_{\alpha\beta\alpha'\beta'}^{(6)}(\vec{r}) = \sum_{\vec{X}} \left([p_\alpha^{(6)}](\vec{X}+\vec{r}) \times [\Lambda_\beta^{(6)}](\vec{X})\right)_{\alpha'\beta'}$$
$$= \sum_{\vec{X}} \sum_{c_2',c_6',\alpha_6'} [p_{\alpha\alpha'\beta'}^{(6)}](\vec{X}+\vec{r}; c_2', c_6', \alpha_6')[\Lambda_\beta^{(6)}](\vec{X}; c_2', c_6', \alpha_6'), \tag{31}$$

where

$$[p_{\alpha\alpha'\beta'}^{(6)}](\vec{x}; c_2', c_6', \alpha_6')$$
$$= \varepsilon(1,4,2)(C\gamma_5)(1,4)\delta(\alpha,2)\delta(\alpha',2')\varepsilon(5',6',3')(C\gamma_5)(5',6')\delta(\beta',3')$$
$$\times \det \begin{vmatrix} \langle u(1)\bar{u}(2')\rangle & \langle u(1)\bar{u}(3')\rangle \\ \langle u(2)\bar{u}(2')\rangle & \langle u(2)\bar{u}(3')\rangle \end{vmatrix} \langle d(4)\bar{d}(5')\rangle, \tag{32}$$
$$[\Lambda_\beta^{(6)}](\vec{y}; c_2', c_6', \alpha_6')$$
$$= \varepsilon(5,6,3)\left\{(C\gamma_5)(5,6)\delta(\beta,3) + (C\gamma_5)(6,3)\delta(\beta,5) - 2(C\gamma_5)(3,5)\delta(\beta,6)\right\}$$
$$\times \varepsilon(1',4',2')(C\gamma_5)(1',4')\langle u(3)\bar{u}(1')\rangle\langle d(5)\bar{d}(4')\rangle\langle s(6)\bar{s}(6')\rangle. \tag{33}$$

Note that the two outer indices $(\alpha'\beta')$ in the source gather into $[p_{\alpha\alpha'\beta'}^{(6)}]$ because the tensorial factors $\varepsilon(5',6',3')(C\gamma_5)(5',6')\delta(\beta',3')$ and $\varepsilon(1',4',2')(C\gamma_5)(1',4')$ are exchanged between $[p_{\alpha\alpha'\beta'}^{(6)}]$ and $[\Lambda_\beta^{(6)}]$ while $\delta(\alpha',2')$ is kept in $[p_{\alpha\alpha'\beta'}^{(6)}]$. The number of explicit summations of indices reduces to two colours and one spinor, which makes the reduction factor $(N_c! N_\alpha)^2 \times 2^{B-N_\Lambda - N_{\Sigma^0}}/(N_c^2 N_\alpha) = 32$.

Performed these manipulations based on the diagrammatic classification, most of the summations can be carried out prior to evaluating the FFT so

that the number of iterations significantly reduces; the numbers of iteration are $\{1, 9, 144, 144, 36, 36\}$ for the baryon blocks $\{([p_\alpha^{(i)}] \times [\Lambda_\beta^{(i)}]); i = 1, \cdots, 6\}$. Therefore only 370 iterations should be explicitly performed to obtain the four-point correlation function of the $p\Lambda$ system when we take the operator $\overline{X}_u$ in $\overline{\Lambda}_{\beta'}$ in the source. For the sake of completeness, the total number of iterations does not change when we take the operator $\overline{X}_s$ in $\overline{\Lambda}_{\beta'}$ in the source whereas the numbers of iteration are $\{1, 36, 36, 144, 144, 36\}$ when we consider the contribution from the operator $\overline{X}_d$ in $\overline{\Lambda}_{\beta'}$ in the source, which slightly differ from the former cases and the total number of iterations is 397.

4. Extension to various BB channels

The effective block algorithm mentioned above is applicable to various BB channels. In the recent few years, the 2+1 flavour lattice QCD calculations have been widely performed. This is an opportune moment to go beyond the BB potentials at the flavour $SU(3)$ point [19] since exploring breakdown of the flavour symmetry is not only an intriguing subject but also a major concern of the phenomenological YN and YY interaction models. Therefore, it is beneficial to take account of a large number of BB channels. For example, we consider the following 52 four-point correlation functions in order to study the complete set of BB interactions in the isospin symmetric limit. (For the moment, we assume that the electromagnetic interaction is not taken into account in the present lattice calculation.)

$$\langle pn\overline{pn}\rangle, \tag{34}$$

$$\begin{aligned}
&\langle p\Lambda\overline{p\Lambda}\rangle, \quad \langle p\Lambda\overline{\Sigma^+n}\rangle, \quad \langle p\Lambda\overline{\Sigma^0p}\rangle, \\
&\langle \Sigma^+n\overline{p\Lambda}\rangle, \quad \langle \Sigma^+n\overline{\Sigma^+n}\rangle, \quad \langle \Sigma^+n\overline{\Sigma^0p}\rangle, \\
&\langle \Sigma^0p\overline{p\Lambda}\rangle, \quad \langle \Sigma^0p\overline{\Sigma^+n}\rangle, \quad \langle \Sigma^0p\overline{\Sigma^0p}\rangle,
\end{aligned} \tag{35}$$

$$\begin{aligned}
&\langle \Lambda\Lambda\overline{\Lambda\Lambda}\rangle, \quad \langle \Lambda\Lambda\overline{p\Xi^-}\rangle, \quad \langle \Lambda\Lambda\overline{n\Xi^0}\rangle, \quad \langle \Lambda\Lambda\overline{\Sigma^+\Sigma^-}\rangle, \quad \langle \Lambda\Lambda\overline{\Sigma^0\Sigma^0}\rangle, \\
&\langle p\Xi^-\overline{\Lambda\Lambda}\rangle, \quad \langle p\Xi^-\overline{p\Xi^-}\rangle, \quad \langle p\Xi^-\overline{n\Xi^0}\rangle, \quad \langle p\Xi^-\overline{\Sigma^+\Sigma^-}\rangle, \quad \langle p\Xi^-\overline{\Sigma^0\Sigma^0}\rangle, \quad \langle p\Xi^-\overline{\Sigma^0\Lambda}\rangle, \\
&\langle n\Xi^0\overline{\Lambda\Lambda}\rangle, \quad \langle n\Xi^0\overline{p\Xi^-}\rangle, \quad \langle n\Xi^0\overline{n\Xi^0}\rangle, \quad \langle n\Xi^0\overline{\Sigma^+\Sigma^-}\rangle, \quad \langle n\Xi^0\overline{\Sigma^0\Sigma^0}\rangle, \quad \langle n\Xi^0\overline{\Sigma^0\Lambda}\rangle, \\
&\langle \Sigma^+\Sigma^-\overline{\Lambda\Lambda}\rangle, \quad \langle \Sigma^+\Sigma^-\overline{p\Xi^-}\rangle, \quad \langle \Sigma^+\Sigma^-\overline{n\Xi^0}\rangle, \quad \langle \Sigma^+\Sigma^-\overline{\Sigma^+\Sigma^-}\rangle, \quad \langle \Sigma^+\Sigma^-\overline{\Sigma^0\Sigma^0}\rangle, \quad \langle \Sigma^+\Sigma^-\overline{\Sigma^0\Lambda}\rangle, \\
&\langle \Sigma^0\Sigma^0\overline{\Lambda\Lambda}\rangle, \quad \langle \Sigma^0\Sigma^0\overline{p\Xi^-}\rangle, \quad \langle \Sigma^0\Sigma^0\overline{n\Xi^0}\rangle, \quad \langle \Sigma^0\Sigma^0\overline{\Sigma^+\Sigma^-}\rangle, \quad \langle \Sigma^0\Sigma^0\overline{\Sigma^0\Sigma^0}\rangle, \\
&\qquad\qquad \langle \Sigma^0\Lambda\overline{p\Xi^-}\rangle, \quad \langle \Sigma^0\Lambda\overline{n\Xi^0}\rangle, \quad \langle \Sigma^0\Lambda\overline{\Sigma^+\Sigma^-}\rangle, \qquad\qquad \langle \Sigma^0\Lambda\overline{\Sigma^0\Lambda}\rangle,
\end{aligned} \tag{36}$$

$$\begin{aligned}
&\langle \Xi^-\Lambda\overline{\Xi^-\Lambda}\rangle, \quad \langle \Xi^-\Lambda\overline{\Sigma^-\Xi^0}\rangle, \quad \langle \Xi^-\Lambda\overline{\Sigma^0\Xi^-}\rangle, \\
&\langle \Sigma^-\Xi^0\overline{\Xi^-\Lambda}\rangle, \quad \langle \Sigma^-\Xi^0\overline{\Sigma^-\Xi^0}\rangle, \quad \langle \Sigma^-\Xi^0\overline{\Sigma^0\Xi^-}\rangle, \\
&\langle \Sigma^0\Xi^-\overline{\Xi^-\Lambda}\rangle, \quad \langle \Sigma^0\Xi^-\overline{\Sigma^-\Xi^0}\rangle, \quad \langle \Sigma^0\Xi^-\overline{\Sigma^0\Xi^-}\rangle,
\end{aligned} \tag{37}$$

$$\langle \Xi^-\Xi^0\overline{\Xi^-\Xi^0}\rangle, \tag{38}$$

13

We omit four off-diagonal channels, $\langle \Lambda\Lambda\overline{\Sigma^0\Lambda}\rangle$, $\langle \Sigma^0\Sigma^0\overline{\Sigma^0\Lambda}\rangle$, $\langle \Sigma^0\Lambda\overline{\Lambda\Lambda}\rangle$ and $\langle \Sigma^0\Lambda\overline{\Sigma^0\Sigma^0}\rangle$, from the above list because they are expected to be identically zero in the isospin symmetric limit [3]. For an extension of the calculation of the four-point correlator to various BB channels, we have implemented a C++ program to perform the Wick contraction together with the FFT in terms of the diagrammatic classification, the procedures of which are automatically performed once the interpolating fields in the source and sink (i.e., the quantum numbers of the system) are given. We also independently implemented another C++ program which performs the Wick contractions to calculate the above 52 channels of four-point correlation function without employing the FFT. We have confirmed that the numerical results obtained by the present effective block algorithm agree with the numerical results calculated by the latter C++ program. See also Sec. 6 for thoroughgoing check between this algorithm and the unified contraction algorithm.

Table 1 lists the number of diagrams, the number of iterations together with the parity of the permutation, and the number of total iterations for the four-point correlation functions of various BB channels with the strangeness $S = 0$ and -1. For the NN system, the number of total iterations for the channel $\langle pn\overline{pn}\rangle$ is just 586, which is quite small in comparison with the $N_{\mathrm{contr}} = 2358$ in Table A.3 in Ref. [29]. As is discussed in the previous section, for the channels with $S = -1$, the numbers of iteration lessened by the effective block algorithm depend on the form of the diquark combination in the baryon field operators in the source. It is therefore convenient to separate between the contributions from the fields $\overline{X}_u$, $\overline{X}_d$, and $\overline{X}_s$ if the correlator comprises the field(s) $\overline{\Lambda}$ and/or $\overline{\Sigma^0}$ in the source. In the Table 1, we explicitly indicate the form of diquark combination such as $\langle p\Lambda\overline{p\Lambda_{X_{u,s}}}\rangle$ and $\langle p\Lambda\overline{p\Lambda_{X_d}}\rangle$ to distinguish the diquark combinations when the correlator includes $\overline{\Lambda}$ and/or $\overline{\Sigma^0}$. Among the numbers of the total iterations for various channels with the strangeness $S = -1$, the largest number is 405 which is found at the channels of $\langle p\Lambda\overline{\Sigma^+ n}\rangle$ and $\langle \Sigma^0 p\overline{\Sigma^+ n}\rangle$; it is noticeably smaller than the smallest value $N_{\mathrm{contr}} = 1350$ (except 0) among the Tables A.1, A.3 and A.5 in Ref. [29].

---

[3] In this paper, we focus on the $2+1$ flavour lattice QCD calculation for the study of the octet-baryon-octet-baryon interactions in the isospin symmetric limit. An extension to the other charge states than the channels given in Eqs. $(34)-(38)$ is straightforward. Moreover, even though the system comprises decuplet baryons such as Ω^-'s, we can take Eq. (11) and the gamma matrices $\Gamma_1 = C\gamma_\ell$ and $\Gamma_2 = 1$ with spatial vector index ℓ.

Because there are a lot of channels for the strangeness $S = -2$, we divide the list into two parts. Table 2 (Table 3) shows the first (second) part of the list of the numbers of iteration for the channels with the strangeness $S = -2$. The five four-point correlation functions, $\langle \Lambda\Lambda\overline{\Lambda_{X_q}\Lambda_{X_{q'}}}\rangle$, $\langle \Lambda\Lambda\overline{\Sigma^0_{X_q}\Sigma^0_{X_{q'}}}\rangle$, $\langle \Sigma^0\Sigma^0\overline{\Lambda_{X_q}\Lambda_{X_{q'}}}\rangle$, $\langle \Sigma^0\Sigma^0\overline{\Sigma^0_{X_q}\Sigma^0_{X_{q'}}}\rangle$, and $\langle \Sigma^0\Lambda\overline{\Sigma^0_{X_q}\Lambda_{X_{q'}}}\rangle$ (for $q = q'$), are the relatively computationally demanding channels in the Tables; the total numbers of iterations are all 596 for these channels and they are remarkably smaller than the any N_{contr} values (except 0) among the Tables A.1, A.3 and A.5 in Ref. [29].

Table 4 shows the numbers of iterations to calculate the four-point correlation functions of the strangeness $S = -3$ and -4 systems. There are similarities in the list of numbers between $S = -3$ and $S = -1$ since the isospin quantum number of Ξ is same as the isospin of N. Therefore the efficiency for the calculation of correlators of $S = -3$ systems is similar to that of $S = -1$ systems. On the other hand, the numbers of iterations to calculate the four-point correlation function of the $S = -4$ system differ from the numbers of iterations to calculate the correlator of the $S = 0$ system. The total number of iterations is 370 for $\langle \Xi^-\Xi^0\overline{\Xi^-\Xi^0}\rangle$ whereas the total number of iterations is 586 for $\langle pn\overline{pn}\rangle$.

5. Hybrid parallel computation of the four-point correlators

The message passing interface (MPI) is a message-passing standard designed for distributed memory parallel computers. In an MPI parallel computation, the communication among distributed computer systems is handled by a communicator object such as `MPI_COMM_WORLD`. Open Multi-Processing (OpenMP) is an application programming interface to control the multi-threading computation on the shared-memory multiprocessor. The master thread forks several slave threads when an OpenMP directive such as "`#pragma omp parallel`" appears in the program; and each thread concurrently executes the computation on the shared memory and finally joins the master thread at the end of the current block. The MPI and OpenMP are basically independent approaches to parallel computation. In recent years, hybrid parallel computing on massive supercomputers such as BlueGene/Q has become inevitable for obtaining a better computational performance.

We develop a hybrid parallel C++ program using both MPI and OpenMP to calculate the four-point correlation functions of various BB channels. The

Table 1: The number of diagrams, the number of iterations together with the parity of the permutation for each diagram, and the number of total iterations for the four-point correlation functions of various BB channels with the strangeness $S = 0$ and -1. See text for details.

channel	# of diagrams	$\{(\text{\# of iterations})^{\text{sign}}\}$	# of total iterations
$\langle pn\overline{pn}\rangle$	9	$\{1^+, 36^-, 144^-, 36^+, 36^+, 144^-, 144^+, 9^-, 36^+\}$	586
$\langle p\Lambda\overline{p\Lambda_{X_{u,s}}}\rangle$	6	$\{1^+, 9^-, 144^-, 144^+, 36^+, 36^-\}$	370
$\langle p\Lambda\overline{p\Lambda_{X_d}}\rangle$	6	$\{1^+, 36^-, 36^-, 144^+, 144^+, 36^-\}$	397
$\langle p\Lambda\overline{\Sigma^+n}\rangle$	6	$\{144^-, 36^+, 36^+, 144^-, 9^-, 36^+\}$	405
$\langle p\Lambda\overline{\Sigma^0_{X_u}p}\rangle$	6	$\{144^+, 36^-, 9^-, 36^+, 144^+, 1^-\}$	370
$\langle p\Lambda\overline{\Sigma^0_{X_d}p}\rangle$	6	$\{144^-, 36^+, 36^+, 144^-, 36^-, 1^+\}$	397
$\langle \Sigma^+n\overline{p\Lambda_{X_u}}\rangle$	3	$\{144^-, 144^+, 36^-\}$	324
$\langle \Sigma^+n\overline{p\Lambda_{X_d}}\rangle$	3	$\{144^-, 36^+, 9^-\}$	189
$\langle \Sigma^+n\overline{p\Lambda_{X_s}}\rangle$	3	$\{36^-, 144^+, 36^-\}$	216
$\langle \Sigma^+n\overline{\Sigma^+n}\rangle$	3	$\{1^+, 36^-, 144^+\}$	181
$\langle \Sigma^+n\overline{\Sigma^0_{X_u}p}\rangle$	3	$\{144^-, 36^+, 144^-\}$	324
$\langle \Sigma^+n\overline{\Sigma^0_{X_d}p}\rangle$	3	$\{36^+, 9^-, 144^+\}$	189
$\langle \Sigma^0p\overline{p\Lambda_{X_{u,s}}}\rangle$	6	$\{36^+, 144^-, 144^+, 36^-, 9^+, 1^-\}$	370
$\langle \Sigma^0p\overline{p\Lambda_{X_d}}\rangle$	6	$\{36^+, 144^-, 36^+, 144^-, 36^+, 1^-\}$	397
$\langle \Sigma^0p\overline{\Sigma^+n}\rangle$	6	$\{36^-, 144^+, 36^-, 9^+, 36^-, 144^+\}$	405
$\langle \Sigma^0p\overline{\Sigma^0_{X_u}p}\rangle$	6	$\{1^+, 36^-, 9^+, 144^-, 36^+, 144^-\}$	370
$\langle \Sigma^0p\overline{\Sigma^0_{X_d}p}\rangle$	6	$\{1^-, 144^+, 36^-, 36^+, 36^-, 144^+\}$	397

program works on general purpose computers such as the BlueGene/Q at the High Energy Accelerator Research Organisation (KEK) and HA-PACS at the University of Tsukuba. In a hybrid parallel computer program, the function `MPI_Init_thread(int* argc, char ***argv, int required, int *provided)` is called instead of `MPI_Init(int* argc, char ***argv)`. For the third argument, we take the `MPI_THREAD_MULTIPLE` together with partitioning the `MPI_COMM_WORLD` into a number of sub-communicators in order to perform the multiple MPI communication through the sub-communicators concurrently from each forked multithreads.

Table 5 shows several elapsed times measured using the 32-node job class of BlueGene/Q at KEK during the calculations of the 52 channels of the four-point correlation functions. The calculations are performed for a gauge configuration provided by CP-PACS and JLQCD Collaboration with a size of $L^3 \times T = 16^3 \times 32$ [35]. Table 5 presents the results of the calculation of the four-point correlation functions and is divided into two parts: the first part shows the data for the calculations of all single baryon blocks together

with its FFT (step-1). From the forms of the baryons' interpolating fields in Eqs. (2), (8)−(9), it turns out that only six (constituents of) single baryon blocks, $B = p, \Sigma^+, \Xi^0, X_u, X_d$, and X_s, are actually computed so that all single baryon blocks, $B = p, n, \Sigma^+, \Sigma^0, \Sigma^-, \Xi^0, \Xi^-$, and Λ, are obtained from the above because of the symmetry under the interchange of the up and down quarks except for the overall phase factors in the isospin symmetric limit. The Second part shows the calculations of the 52 four-point correlation functions $\sum_{\vec{X}} \left\langle B_{1,\alpha}(\vec{X} + \vec{r}, t) B_{2,\beta}(\vec{X}, t) \overline{\mathcal{J}_{B_{3,\alpha'} B_{4,\beta'}}(0)} \right\rangle$, $(t = 0, \cdots, T - 1)$ from the baryon blocks by performing the summations of the indices of colour and spinor together with its inverse FFT (step-2). The elapsed time is measured for various combinations of the number of MPI processes (`tasks_per_node`) and the number of threads (`OMP_NUM_THREADS`). The elapsed time indicated by "64×1" is obtained from the so-called flat-MPI calculation. Sometimes, during hybrid parallel computations, there is a problem that hybrid parallel executions are not faster than the flat-MPI calculation. Our calculations do not show such a behaviour and the present program exhibits almost stable and reasonable performances for various combinations of the number of MPI processes and the number of threads.

In step-1, the memory size can be reduced by sharing the memory of each baryon block if the same diagram appears (i.e. the components are numerically equivalent) throughout the 52 channels of the BB four-point correlation functions. At present, this provides a benefit only for the memory usage, because computational cost of mapping the sharing of baryon blocks nullifies the gain in timing performance (see Appendix A for further details).

6. Benchmark with the unified contraction algorithm

In order to see the correctness of the present implementation of the effective block algorithm developed in Sec. 5, we benchmarked the numerical output with the corresponding data from the unified contraction algorithm [29]. The benchmark has been done by using a gauge configuration provided from CP-PACS and JLQCD Collaboration with a size of $L^3 \times T = 16^3 \times 32$ [35]. We have used a wall quark source with Coulomb gauge fixing and the periodic (Dirichlet) boundary condition has been imposed in the spatial (temporal) direction. Table 6 shows just 16 lines of the comparisons as an example. For the correlator $R_{\alpha\beta\alpha'\beta'}(\vec{r}, t - t_0)$ in the low-energy states, we adopt the Dirac representation and calculate upper (lower)

two components of each spinor index to see the positive (negative) parity states of each single baryon (antibaryon) in the forward (backward) direction in time. Because of equivalence between the baryon-baryon states in forward direction in time and the antibaryon-antibaryon states in backward direction in time under the charge conjugation, parity, and time reversal operations, we effectively double our Monte Carlo samples by taking the data in both the forward and backward directions in time. We then reallocate the spinor indices, from $(\alpha, \beta, \alpha', \beta')$ to $(\tilde{\alpha}, \tilde{\beta}, \tilde{\alpha}', \tilde{\beta}')$, to run 0 to 1 for both cases in the numerical computation. The left panel of Figure 2 shows the relative difference, $|\frac{\text{Diff}}{\text{This work}}|$, of the correlator $\sum_{\vec{X}} \left\langle p_\alpha(\vec{X} + \vec{r}, t)\Lambda_\beta(\vec{X}, t)\overline{\mathcal{J}_{p_{\alpha'}\Lambda_{\beta'}}(t_0)} \right\rangle$ at $t - t_0 = 10$, between this effective block algorithm and the unified contraction algorithm as a function of one-dimensionally aligned data point $\xi = \tilde{\alpha} + 2(\tilde{\beta} + 2(\tilde{\alpha}' + 2(\tilde{\beta}' + 2(x + 16(y + 16(z))))))$; there are $16^3 \times 2^4 = 65,536$ data points per time-slice per channel. The comparison is performed for all 52 channels over 31 time-slices, 16^3 points for spatial, and 2^4 points for the spin degrees of freedom. The right panel of Fig. 2 shows the result of the entire comparison between the effective block algorithm and the unified contraction algorithm, as a function of one-dimensionally aligned data point $\xi = \tilde{\alpha} + 2(\tilde{\beta} + 2(\tilde{\alpha}' + 2(\tilde{\beta}' + 2(x + 16(y + 16(z + 16(c + 52((t - t_0 + T) \bmod T)))))))))$, where $c = 0, \cdots, 51$ selects one of 52 channels given in Eqs. $(34) - (38)$[4]. All numerical results are in good agreement with an accuracy of almost the double precision.

7. Summary

In this paper, we present an approach for the efficient simultaneous calculation of a large number of four-point correlation functions, which are the primary quantities for studying the nuclear and hyperonic nuclear forces from lattice QCD. The effective block algorithm significantly reduces the number of iterations required for the Wick contraction, and is applied to calculate

---

[4] The correlator, $\sum_{\vec{x}}\langle B_{1,\alpha}(\vec{x} + \vec{r})B_{2,\beta}(\vec{x})\overline{B_{3,\alpha'}B_{4,\beta'}}\rangle$, vanishes due to the anticommutation relation of the baryon fields when two baryon fields become identical. It occurs in the following cases, (i) for the identical two baryons in the sink, $B_{1,\alpha} = B_{2,\beta}$, the correlator vanishes at $\vec{r} = $ a cyclic permutation of $(0,0,0), (L/2,0,0), (L/2,L/2,0)$, or $(L/2,L/2,L/2)$ under spatially periodic boundary conditions, (ii) for the identical two baryons in the source, $\overline{B}_{3,\alpha'} = \overline{B}_{4,\beta'}$, the correlator vanishes under the present choice of wall quark source fields. These vanishing data points are not included in the figure.

the 52 channels of four-point correlation functions in order to study the complete set of BB interactions in the isospin symmetric limit. The elapsed time is measured for hybrid parallel computation on the BlueGene/Q supercomputer. The hybrid parallel executions of the $16^3 \times 32$ lattice show reasonable performances for various combinations of the number of MPI processes and the number of threads. The numerical values of the calculated 52 four-point correlation functions are compared with the results obtained using the unified contraction algorithm. We find that all numerical results are in good agreement and the two different algorithms give virtually identical results. This is advantageous for performing the large scale computation of various BB potentials at the physical quark mass point.

Appendix A. The aggregation of effective blocks

When calculating a large number of four-point correlation functions such as 52 channels of NBS wave functions simultaneously, we can economise on computer resource by aggregating the same effective blocks which appear several times through the whole calculation. In this section, we show how the aggregations are performed by considering the explicit form of the $\langle \Sigma^+ n \overline{\Sigma^+ n} \rangle$ correlator.

Appendix A.1. Explicit form of the $\langle \Sigma^+ n \overline{\Sigma^+ n} \rangle$ correlator

The result of diagrammatic classification of the $\langle \Sigma^+ n \overline{\Sigma^+ n} \rangle$ correlator is found in Table 1. We show the explicit forms of the baryon blocks in this

channel. The four-point correlator is given by

$$
\begin{aligned}
& \sum_{\vec{X}} \left\langle 0 \left| \Sigma_\alpha^+(\vec{X}+\vec{r},t)n_\beta(\vec{X},t)\overline{\mathcal{J}_{\Sigma_{\alpha'}^+,n_{\beta'}}(t_0)} \right| 0 \right\rangle \\
= & \sum_{\vec{X}} \varepsilon(1,6,2)\varepsilon(3,4,5)\varepsilon(1',6',2')\varepsilon(3',4',5') \\
& \times (C\gamma_5)(1,6)\delta(\alpha,2)(C\gamma_5)(3,4)\delta(\beta,5)(C\gamma_5)(1',6')\delta(\alpha',2')(C\gamma_5)(3',4')\delta(\beta',5') \\
& \times \langle u(1)s(6)u(2)u(3)d(4)d(5)\bar{d}(5')\bar{d}(4')\bar{u}(3')\bar{u}(2')\bar{s}(6')\bar{u}(1')\rangle,
\end{aligned}
\tag{A.1}
$$

where
$$
\vec{x}_1 = \vec{x}_2 = \vec{x}_6 = \vec{X}+\vec{r}, \qquad \vec{x}_3 = \vec{x}_4 = \vec{x}_5 = \vec{X}. \tag{A.2}
$$

We have suppressed the explicit summations for the indices of colour and spinor in the right hand side. The last line in Eq. (A.1) is Wick contracted and represented in terms of the quark propagators,

$$
\begin{aligned}
& \langle u(1)s(6)u(2)u(3)d(4)d(5)\bar{d}(5')\bar{d}(4')\bar{u}(3')\bar{u}(2')\bar{s}(6')\bar{u}(1')\rangle \\
= & \left\{ \langle u(3)\bar{u}(3')\rangle \det \begin{vmatrix} \langle u(1)\bar{u}(1')\rangle & \langle u(1)\bar{u}(2')\rangle \\ \langle u(2)\bar{u}(1')\rangle & \langle u(2)\bar{u}(2')\rangle \end{vmatrix} \right. \\
& - \langle u(3)\bar{u}(2')\rangle \det \begin{vmatrix} \langle u(1)\bar{u}(1')\rangle & \langle u(1)\bar{u}(3')\rangle \\ \langle u(2)\bar{u}(1')\rangle & \langle u(2)\bar{u}(3')\rangle \end{vmatrix} \\
& \left. + \langle u(3)\bar{u}(1')\rangle \det \begin{vmatrix} \langle u(1)\bar{u}(2')\rangle & \langle u(1)\bar{u}(3')\rangle \\ \langle u(2)\bar{u}(2')\rangle & \langle u(2)\bar{u}(3')\rangle \end{vmatrix} \right\} \\
& \times \det \begin{vmatrix} \langle d(4)\bar{d}(4')\rangle & \langle d(4)\bar{d}(5')\rangle \\ \langle d(5)\bar{d}(4')\rangle & \langle d(5)\bar{d}(5')\rangle \end{vmatrix} \langle s(6)\bar{s}(6')\rangle.
\end{aligned}
\tag{A.3}
$$

Fig. A.3 shows the diagrammatic representation of the correlator $\langle \Sigma^+ n\overline{\Sigma^+ n}\rangle$. The four-point correlation function is calculated using the FFT. We show the explicit forms of the three baryon-block pairs $\left([\Sigma_\alpha^{+(1)}] \times [n_\beta^{(1)}]\right)$, $\left([\Sigma_\alpha^{+(2)}] \times [n_\beta^{(2)}]\right)$, $\left([\Sigma_\alpha^{+(3)}] \times [n_\beta^{(3)}]\right)$.

(i) $\Sigma_\alpha^{+(1)}$ and $n_\beta^{(1)}$
  This is a product of two two-point correlators.

$$
R_{\alpha\beta\alpha'\beta'}^{(1)}(\vec{r}) = \sum_{\vec{X}} \left([\Sigma_\alpha^{+(1)}](\vec{X}+\vec{r}) \times [n_\beta^{(1)}](\vec{X})\right)_{\alpha'\beta'} = \sum_{\vec{X}} [\Sigma_{\alpha\alpha'}^{+(1)}](\vec{X}+\vec{r})[n_{\beta\beta'}^{(1)}](\vec{X}),
\tag{A.4}
$$

20

where

$$[\Sigma^{+\,(1)}_{\alpha\alpha'}](\vec{x}) = \varepsilon(1,6,2)(C\gamma_5)(1,6)\delta(\alpha,2)\varepsilon(1',6',2')(C\gamma_5)(1',6')\delta(\alpha',2')$$

$$\times \det \begin{vmatrix} \langle u(1)\bar{u}(1')\rangle & \langle u(1)\bar{u}(2')\rangle \\ \langle u(2)\bar{u}(1')\rangle & \langle u(2)\bar{u}(2')\rangle \end{vmatrix} \langle s(6)\bar{s}(6')\rangle, \tag{A.5}$$

$$\left[n^{(1)}_{\beta\beta'}\right](\vec{y}) = \varepsilon(3,4,5)(C\gamma_5)(3,4)\delta(\beta,5)\varepsilon(3',4',5')(C\gamma_5)(3',4')\delta(\beta',5')$$

$$\times\langle u(3)\bar{u}(3')\rangle \det \begin{vmatrix} \langle d(4)\bar{d}(4')\rangle & \langle d(4)\bar{d}(5')\rangle \\ \langle d(5)\bar{d}(4')\rangle & \langle d(5)\bar{d}(5')\rangle \end{vmatrix}. \tag{A.6}$$

All of the summation of internal indices $(\sum_{c_1,\cdots,c_6} \sum_{c'_1,\cdots,c'_6} \sum_{\alpha_1,\cdots,\alpha_6} \sum_{\alpha'_1,\cdots,\alpha'_6})$ can be performed separately for $[\Sigma^{+\,(1)}_{\alpha\alpha'}]$ and $\left[n^{(1)}_{\beta\beta'}\right]$.

(ii) $\boldsymbol{\Sigma^{+(2)}_{\alpha}}$ **and** $\boldsymbol{n^{(2)}_{\beta}}$

This is an one-quark exchange diagram.

$$R^{(2)}_{\alpha\beta\alpha'\beta'}(\vec{r}) = \sum_{\vec{X}} \left([\Sigma^{+(2)}_{\alpha}](\vec{X}+\vec{r}) \times [n^{(2)}_{\beta}](\vec{X})\right)_{\alpha'\beta'}$$

$$= \sum_{\vec{X}} \sum_{c'_2,c'_3,\alpha'_3} [\Sigma^{+(2)}_{\alpha}](\vec{X}+\vec{r}; c'_2, c'_3, \alpha'_3)[n^{(2)}_{\beta\alpha'\beta'}](\vec{X}; c'_2, c'_3, \alpha'_3), \tag{A.7}$$

where

$$[\Sigma^{+(2)}_{\alpha}](\vec{x}; c'_2, c'_3, \alpha'_3)$$
$$= \varepsilon(1,6,2)(C\gamma_5)(1,6)\delta(\alpha,2)\varepsilon(1',6',2')(C\gamma_5)(1',6')$$

$$\times \det \begin{vmatrix} \langle u(1)\bar{u}(1')\rangle & \langle u(1)\bar{u}(3')\rangle \\ \langle u(2)\bar{u}(1')\rangle & \langle u(2)\bar{u}(3')\rangle \end{vmatrix} \langle s(6)\bar{s}(6')\rangle, \tag{A.8}$$

$$[n^{(2)}_{\beta\alpha'\beta'}](\vec{y}; c'_2, c'_3, \alpha'_3)$$
$$= \varepsilon(3,4,5)(C\gamma_5)(3,4)\delta(\beta,5)\varepsilon(3',4',5')(C\gamma_5)(3',4')\delta(\beta',5')\delta(\alpha',2')$$

$$\times\langle u(3)\bar{u}(2')\rangle \det \begin{vmatrix} \langle d(4)\bar{d}(4')\rangle & \langle d(4)\bar{d}(5')\rangle \\ \langle d(5)\bar{d}(4')\rangle & \langle d(5)\bar{d}(5')\rangle \end{vmatrix}. \tag{A.9}$$

We have additional arguments (c'_2, c'_3, α'_3) for the baryon blocks $[\Sigma^{+(2)}_{\alpha}]$ and $[n^{(2)}_{\beta}]$ because of the exchange of u-quark in the source. Note that the summation of α'_2 can be always omitted because of the presence of $\delta(\alpha',2')$ located in $[n^{(2)}_{\beta}]$.

21

(iii) $\boldsymbol{\Sigma_\alpha^{+(3)}}$ and $\boldsymbol{n_\beta^{(3)}}$

This is another exchange diagram.

$$R^{(3)}_{\alpha\beta\alpha'\beta'}(\vec{r}) = \sum_{\vec{X}} \left([\Sigma_\alpha^{+(3)}](\vec{X}+\vec{r}) \times [n_\beta^{(3)}](\vec{X}) \right)_{\alpha'\beta'}$$

$$= \sum_{\vec{X}} \sum_{c_1',c_3',\alpha_1',\alpha_3'} [\Sigma_{\alpha\alpha'}^{+(3)}](\vec{X}+\vec{r}; c_1', c_3', \alpha_1', \alpha_3')[n_{\beta\beta'}^{(3)}](\vec{X}; c_1', c_3', \alpha_1', \alpha_3') \quad (A.10)$$

where

$$[\Sigma_{\alpha\alpha'}^{+\ (3)}](\vec{x}; c_1', c_3', \alpha_1', \alpha_3')$$
$$= \ \varepsilon(1,6,2)(C\gamma_5)(1,6)\delta(\alpha,2)\varepsilon(1',6',2')(C\gamma_5)(1',6')\delta(\alpha',2')$$
$$\times \det \begin{vmatrix} \langle u(1)\bar{u}(2')\rangle & \langle u(1)\bar{u}(3')\rangle \\ \langle u(2)\bar{u}(2')\rangle & \langle u(2)\bar{u}(3')\rangle \end{vmatrix} \langle s(6)\bar{s}(6')\rangle, \quad (A.11)$$

$$[n_{\beta\beta'}^{(3)}](\vec{y}; c_1', c_3', \alpha_1', \alpha_3')$$
$$= \ \varepsilon(3,4,5)(C\gamma_5)(3,4)\delta(\beta,5)\varepsilon(3',4',5')(C\gamma_5)(3',4')\delta(\beta',5')$$
$$\times \langle u(3)\bar{u}(1')\rangle \det \begin{vmatrix} \langle d(4)\bar{d}(4')\rangle & \langle d(4)\bar{d}(5')\rangle \\ \langle d(5)\bar{d}(4')\rangle & \langle d(5)\bar{d}(5')\rangle \end{vmatrix}. \quad (A.12)$$

Appendix A.2. Finding reusable baryon blocks

In the isospin symmetric limit, the single neutron correlator in Eq. (A.6) is identical with the single proton correlator in Eq. (17) because the interpolating fields of proton and neutron in Eq. (2) are symmetric under the interchange of the up and down quarks except for the overall phase factors. Thus we may avoid the actual numerical calculation of the $[n_{\beta\beta'}^{(1)}](\vec{y})$ in $\langle \Sigma^+ n\ \overline{\Sigma^+ n} \rangle$ by using the result of $[p_{\alpha\alpha'}^{(1)}](\vec{x})$ in $\langle p\Lambda\overline{p\Lambda}\rangle$ instead:

$$[n_{\beta\beta'}^{(1)}](\vec{y})_{\langle \Sigma^+ n\ \overline{\Sigma^+ n} \rangle} = \left([p_{\alpha\alpha'}^{(1)}](\vec{x})_{\langle p\Lambda\overline{p\Lambda}\rangle} \right) \begin{pmatrix} \alpha \to \beta \\ \alpha' \to \beta' \\ \vec{x} \to \vec{y} \end{pmatrix}. \quad (A.13)$$

The usage of Eq. (A.13) gives right result provided that the spatial reflection in momentum space is taken into account when performing the FFT with the replacement of the space coordinate $\vec{x} \to \vec{y}$. See Eq. (15), where the argument of the second baryon is $(-\vec{q})$ while the first baryon serves $(\vec{q})$. The above first example might be a very trivial case. The second example is to

22

find that the $[n_\beta^{(2)}](\vec{y})$ in $\langle\,\Sigma^+ n\,\overline{\Sigma^+ n}\,\rangle$ in Eq. (A.9) is a special case of $[n_\beta^{(3)}](\vec{y})$ in $\langle\,\Sigma^+ n\,\overline{\Sigma^+ n}\,\rangle$ in Eq. (A.12),

$$[n_{\beta\alpha'\beta'}^{(2)}](\vec{y}; c_2', c_3', \alpha_3')_{\langle\Sigma^+ n\overline{\Sigma^+ n}\rangle} = \left([n_{\beta\beta'}^{(3)}](\vec{y}; c_1', c_3', \alpha_1', \alpha_3')_{\langle\Sigma^+ n\overline{\Sigma^+ n}\rangle}\right)_{\left(\begin{array}{c} c_1' \to c_2' \\ \alpha_1' \to \alpha_2' = \alpha' \end{array}\right)}.$$

(A.14)

These kinds of reusable baryon blocks can be found in various parts in the entire 52 channels of the NBS wave functions. We list only a few more examples that figuring in one's head is possible from the above explicit forms of the baryon blocks shown in this paper:

$$[n_{\beta\beta'}^{(3)}](\vec{y}; c_1', c_3', \alpha_1', \alpha_3')_{\langle\Sigma^+ n\overline{\Sigma^+ n}\rangle} = \left([p_{\alpha\alpha'}^{(4)}](\vec{x}; c_4', c_5', \alpha_4', \alpha_5')_{\langle p\Lambda\overline{p\Lambda}\rangle}\right)_{\left(\begin{array}{c} (c_4', \alpha_4') \to (c_3', \alpha_3') \\ (c_5', \alpha_5') \to (c_1', \alpha_1') \\ \alpha \to \beta \\ \alpha' \to \beta' \\ \vec{x} \to \vec{y} \end{array}\right)},$$

(A.15)

$$[p_{\alpha\alpha'\beta'}^{(6)}](\vec{x}; c_2', c_6', \alpha_6')_{\langle p\Lambda\overline{p\Lambda}\rangle} = \left([p_{\alpha\beta'}^{(4)}](\vec{x}; c_1', c_6', \alpha_1', \alpha_6')_{\langle p\Lambda\overline{p\Lambda}\rangle}\right)_{\left(\begin{array}{c} c_1' \to c_2' \\ \alpha_1' \to \alpha_2' = \alpha' \end{array}\right)},$$

(A.16)

$$[\Lambda_{\beta\alpha'}^{(2)}](\vec{y}; c_2', c_3')_{\langle p\Lambda\overline{pX_u}\rangle} = \left([\Lambda_\beta^{(5)}](\vec{y}; c_1', c_3', \alpha_1')_{\langle p\Lambda\overline{pX_u}\rangle}\right)_{\left(\begin{array}{c} c_1' \to c_2' \\ \alpha_1' \to \alpha_2' = \alpha' \end{array}\right)}.$$

(A.17)

Table A.7 summarises that how the memory size reduces by considering the aggregations of the effective baryon blocks throughout the entire 52 channels of the NBS wave functions.

References

[1] R. Machleidt, Phys. Rev. C **63**, 024001 (2001) [nucl-th/0006014].

[2] M. M. Nagels, T. A. Rijken and J. J. de Swart, Phys. Rev. D **20**, 1633 (1979).

[3] S. C. Pieper, V. R. Pandharipande, R. B. Wiringa and J. Carlson, Phys. Rev. C **64**, 014001 (2001) [nucl-th/0102004].

[4] A. Nogga, H. Kamada, W. Gloeckle and B. R. Barrett, Phys. Rev. C **65**, 054003 (2002) [nucl-th/0112026].

[5] H. Nemura, Y. Akaishi and Y. Suzuki, Phys. Rev. Lett. **89**, 142504 (2002) [arXiv:nucl-th/0203013].

[6] A. Nogga, H. Kamada and W. Gloeckle, Phys. Rev. Lett. **88**, 172501 (2002) [nucl-th/0112060].

[7] T. O. Yamamoto *et al.* [J-PARC E13-1st Collaboration], arXiv:1508.00376 [nucl-ex].

[8] See e.g. J. Schaffner-Bielich, Nucl. Phys. A **804**, 309 (2008) [arXiv:0801.3791 [astro-ph]].

[9] P. B. Demorest, *et al.*, Nature **467**, 1081 (2010).

[10] J. Antoniadis *et al.*, Science **340**, 6131 (2013) doi:10.1126/science.1233232 [arXiv:1304.6875 [astro-ph.HE]].

[11] K. Masuda, T. Hatsuda and T. Takatsuka, PTEP **2013**, no. 7, 073D01 (2013) [arXiv:1212.6803 [nucl-th]].

[12] N. Ishii, S. Aoki and T. Hatsuda, Phys. Rev. Lett. **99**, 022001 (2007) doi:10.1103/PhysRevLett.99.022001 [nucl-th/0611096].

[13] S. Aoki, T. Hatsuda and N. Ishii, Prog. Theor. Phys. **123**, 89 (2010) doi:10.1143/PTP.123.89 [arXiv:0909.5585 [hep-lat]].

[14] K. Murano, N. Ishii, S. Aoki and T. Hatsuda, Prog. Theor. Phys. **125**, 1225 (2011) doi:10.1143/PTP.125.1225 [arXiv:1103.0619 [hep-lat]].

[15] H. Nemura, N. Ishii, S. Aoki and T. Hatsuda, Phys. Lett. B **673**, 136 (2009) doi:10.1016/j.physletb.2009.02.003 [arXiv:0806.1094 [nucl-th]].

[16] T. Inoue *et al.* [HAL QCD Collaboration], Prog. Theor. Phys. **124**, 591 (2010) doi:10.1143/PTP.124.591 [arXiv:1007.3559 [hep-lat]].

[17] T. Inoue *et al.* [HAL QCD Collaboration], Phys. Rev. Lett. **106**, 162002 (2011) doi:10.1103/PhysRevLett.106.162002 [arXiv:1012.5928 [hep-lat]].

[18] T. Doi *et al.* [HAL QCD Collaboration], Prog. Theor. Phys. **127**, 723 (2012) [arXiv:1106.2276 [hep-lat]].

[19] T. Inoue *et al.* [HAL QCD Collaboration], Nucl. Phys. A **881**, 28 (2012) [arXiv:1112.5926 [hep-lat]].

[20] N. Ishii *et al.* [HAL QCD Collaboration], Phys. Lett. B **712**, 437 (2012) [arXiv:1203.3642 [hep-lat]].

[21] T. Inoue *et al.* [HAL QCD Collaboration], Phys. Rev. Lett. **111**, 112503 (2013) [arXiv:1307.0299 [hep-lat]].

[22] K. Murano *et al.* [HAL QCD Collaboration], Phys. Lett. B **735**, 19 (2014) [arXiv:1305.2293 [hep-lat]].

[23] F. Etminan *et al.* [HAL QCD Collaboration], Nucl. Phys. A **928**, 89 (2014) [arXiv:1403.7284 [hep-lat]].

[24] T. Inoue *et al.* [HAL QCD Collaboration], Phys. Rev. C **91**, no. 1, 011001 (2015) [arXiv:1408.4892 [hep-lat]].

[25] M. Yamada *et al.* [HAL QCD Collaboration], PTEP **2015**, no. 7, 071B01 (2015) [arXiv:1503.03189 [hep-lat]].

[26] S. Aoki *et al.* [HAL QCD Collaboration], Proc. Jpn. Acad. B **87**, 509 (2011) [arXiv:1106.2281 [hep-lat]].

[27] S. Aoki, B. Charron, T. Doi, T. Hatsuda, T. Inoue and N. Ishii, Phys. Rev. D **87**, no. 3, 034512 (2013) [arXiv:1212.4896 [hep-lat]].

[28] K. Sasaki *et al.* [HAL QCD Collaboration], PTEP **2015**, no. 11, 113B01 (2015) doi:10.1093/ptep/ptv144 [arXiv:1504.01717 [hep-lat]].

[29] T. Doi and M. G. Endres, Comput. Phys. Commun. **184**, 117 (2013) [arXiv:1205.0585 [hep-lat]].

[30] H. Nemura, N. Ishii, S. Aoki and T. Hatsuda [PACS-CS Collaboration], PoS **LATTICE2008**, 156 (2008) [arXiv:0902.1251 [hep-lat]].

[31] H. Nemura [HAL QCD Collaboration and PACS-CS Collaboration], PoS **LAT2009**, 152 (2009) [arXiv:1005.5352 [hep-lat]].

[32] H. Nemura [for HAL QCD Collaboration], PoS LATTICE **2011**, 167 (2011) [arXiv:1203.3320 [hep-lat]].

[33] W. Detmold and K. Orginos, Phys. Rev. D **87**, no. 11, 114512 (2013) [arXiv:1207.1452 [hep-lat]].

[34] J. Günther, B. C. Toth and L. Varnhorst, Phys. Rev. D **87**, no. 9, 094513 (2013) [arXiv:1301.4895 [hep-lat]].

[35] T. Ishikawa *et al.* [JLQCD Collaboration], Phys. Rev. D **78**, 011502 (2008) doi:10.1103/PhysRevD.78.011502 [arXiv:0704.1937 [hep-lat]].

[36] See `http://www.lqcd.org/ildg` and `http://www.jldg.org`

[37] Lattice QCD code Bridge++, `http://bridge.kek.jp/Lattice-code/index_e.html`.

[38] Columbia Physics System (CPS), `http://qcdoc.phys.columbia.edu/cps.html`.

Table 2: Same as Table 1 but for the first part of channels with the strangeness $S = -2$.

channel	# of diagrams	$\{(\text{\# of iterations})^{\text{sign}}\}$	# of total iterations
$\langle\Lambda\Lambda\overline{\Lambda_{X_q}\Lambda_{X_{q'}}}\rangle$ $(q=q')$	8	$\{1^+, 9^-, 144^-, 144^+, 144^-, 144^+, 9^+, 1^-\}$	596
$\langle\Lambda\Lambda\overline{\Lambda_{X_q}\Lambda_{X_{q'}}}\rangle$ $(q\neq q')$	8	$\{1^+, 36^-, 144^-, 36^+, 36^-, 144^+, 36^+, 1^-\}$	434
$\langle\Lambda\Lambda\overline{p\Xi^-}\rangle$	8	$\{36^+, 144^-, 9^-, 36^+, 36^-, 9^+, 144^+, 36^-\}$	450
$\langle\Lambda\Lambda\overline{n\Xi^0}\rangle$	8	$\{36^+, 36^-, 9^-, 144^+, 144^-, 9^+, 36^+, 36^-\}$	450
$\langle\Lambda\Lambda\overline{\Sigma^+\Sigma^-}\rangle$	8	$\{36^-, 144^+, 36^+, 9^-, 9^+, 36^-, 144^-, 36^+\}$	450
$\langle\Lambda\Lambda\overline{\Sigma^0_{X_q}\Sigma^0_{X_{q'}}}\rangle$ $(q=q')$	8	$\{1^+, 9^-, 144^-, 144^+, 144^-, 144^+, 9^+, 1^-\}$	596
$\langle\Lambda\Lambda\overline{\Sigma^0_{X_q}\Sigma^0_{X_{q'}}}\rangle$ $(q\neq q')$	8	$\{1^-, 36^+, 144^+, 36^-, 36^+, 144^-, 36^-, 1^+\}$	434
$\langle p\Xi^-\overline{\Lambda_{X_q}\Lambda_{X_q}}\rangle$ $(q=u,s)$	2	$\{36^+, 36^-\}$	72
$\langle p\Xi^-\overline{\Lambda_{X_q}\Lambda_{X_{q'}}}\rangle$ $((q,q')=(d,u),(u,d),(s,d),(d,s))$	2	$\{36^+, 144^-\}$	180
$\langle p\Xi^-\overline{\Lambda_{X_q}\Lambda_{X_{q'}}}\rangle$ $((q,q')=(s,u),(u,s))$	2	$\{9^+, 144^-\}$	153
$\langle p\Xi^-\overline{\Lambda_{X_d}\Lambda_{X_d}}\rangle$	2	$\{144^+, 144^-\}$	288
$\langle p\Xi^-\overline{p\Xi^-}\rangle$	2	$\{1^+, 144^-\}$	145
$\langle p\Xi^-\overline{n\Xi^0}\rangle$	2	$\{36^+, 144^-\}$	180
$\langle p\Xi^-\overline{\Sigma^+\Sigma^-}\rangle$	2	$\{144^-, 36^+\}$	180
$\langle p\Xi^-\overline{\Sigma^0_{X_u}\Sigma^0_{X_u}}\rangle$	2	$\{36^+, 36^-\}$	72
$\langle p\Xi^-\overline{\Sigma^0_{X_q}\Sigma^0_{X_{q'}}}\rangle$ $(q\neq q')$	2	$\{36^-, 144^+\}$	180
$\langle p\Xi^-\overline{\Sigma^0_{X_d}\Sigma^0_{X_d}}\rangle$	2	$\{144^+, 144^-\}$	288
$\langle p\Xi^-\overline{\Sigma^0_{X_u}\Lambda_{X_u}}\rangle$	2	$\{36^+, 36^-\}$	72
$\langle p\Xi^-\overline{\Sigma^0_{X_q}\Lambda_{X_{q'}}}\rangle$ $((q,q')=(d,u),(u,d),(d,s))$	2	$\{36^-, 144^+\}$	180
$\langle p\Xi^-\overline{\Sigma^0_{X_d}\Lambda_{X_d}}\rangle$	2	$\{144^-, 144^+\}$	288
$\langle p\Xi^-\overline{\Sigma^0_{X_u}\Lambda_{X_s}}\rangle$	2	$\{144^+, 9^-\}$	153
$\langle n\Xi^0\overline{\Lambda_{X_u}\Lambda_{X_u}}\rangle$	2	$\{144^+, 144^-\}$	288
$\langle n\Xi^0\overline{\Lambda_{X_q}\Lambda_{X_{q'}}}\rangle$ $((q,q')=(d,u),(u,d),(s,u),(u,s))$	2	$\{144^+, 36^-\}$	180
$\langle n\Xi^0\overline{\Lambda_{X_q}\Lambda_{X_q}}\rangle$ $(q=d,s)$	2	$\{36^+, 36^-\}$	72
$\langle n\Xi^0\overline{\Lambda_{X_q}\Lambda_{X_{q'}}}\rangle$ $((q,q')=(s,d),(d,s))$	2	$\{9^+, 144^-\}$	153
$\langle n\Xi^0\overline{p\Xi^-}\rangle$	2	$\{36^+, 144^-\}$	180
$\langle n\Xi^0\overline{n\Xi^0}\rangle$	2	$\{1^+, 144^-\}$	145
$\langle n\Xi^0\overline{\Sigma^+\Sigma^-}\rangle$	2	$\{144^-, 36^+\}$	180
$\langle n\Xi^0\overline{\Sigma^0_{X_u}\Sigma^0_{X_u}}\rangle$	2	$\{144^+, 144^-\}$	288
$\langle n\Xi^0\overline{\Sigma^0_{X_q}\Sigma^0_{X_{q'}}}\rangle$ $(q\neq q')$	2	$\{144^-, 36^+\}$	180
$\langle n\Xi^0\overline{\Sigma^0_{X_d}\Sigma^0_{X_d}}\rangle$	2	$\{36^+, 36^-\}$	72
$\langle n\Xi^0\overline{\Sigma^0_{X_u}\Lambda_{X_u}}\rangle$	2	$\{144^+, 144^-\}$	288
$\langle n\Xi^0\overline{\Sigma^0_{X_q}\Lambda_{X_{q'}}}\rangle$ $((q,q')=(d,u),(u,d),(u,s))$	2	$\{144^-, 36^+\}$	180
$\langle n\Xi^0\overline{\Sigma^0_{X_d}\Lambda_{X_d}}\rangle$	2	$\{36^-, 36^+\}$	72
$\langle n\Xi^0\overline{\Sigma^0_{X_d}\Lambda_{X_s}}\rangle$	2	$\{144^-, 9^+\}$	153

27

Table 3:   Same as Table 1 but for the second part of channels with the strangeness $S = -2$.

channel	# of diagrams	$\{(\# \text{ of iterations})^{\text{sign}}\}$	# of total iterations
$\langle \Sigma^+\Sigma^-\overline{\Lambda_{X_q}\Lambda_{X_q}}\rangle$ $(q = u, d)$	2	$\{36^-, 36^+\}$	72
$\langle \Sigma^+\Sigma^-\overline{\Lambda_{X_q}\Lambda_{X_{q'}}}\rangle$ $((q,q')=(d,u),(u,d))$	2	$\{9^-, 144^+\}$	153
$\langle \Sigma^+\Sigma^-\overline{\Lambda_{X_q}\Lambda_{X_{q'}}}\rangle$ $((q,q')=(s,u),(s,d),(u,s),(d,s))$	2	$\{36^-, 144^+\}$	180
$\langle \Sigma^+\Sigma^-\overline{\Lambda_{X_s}\Lambda_{X_s}}\rangle$	2	$\{144^-, 144^+\}$	288
$\langle \Sigma^+\Sigma^-\overline{p\Xi^-}\rangle$	2	$\{144^-, 36^+\}$	180
$\langle \Sigma^+\Sigma^-\overline{n\Xi^0}\rangle$	2	$\{36^-, 144^+\}$	180
$\langle \Sigma^+\Sigma^-\overline{\Sigma^+\Sigma^-}\rangle$	2	$\{1^+, 144^-\}$	145
$\langle \Sigma^+\Sigma^-\overline{\Sigma^0_{X_q}\Sigma^0_{X_q}}\rangle$ $(q = u, d)$	2	$\{36^-, 36^+\}$	72
$\langle \Sigma^+\Sigma^-\overline{\Sigma^0_{X_q}\Sigma^0_{X_{q'}}}\rangle$ $(q \neq q')$	2	$\{9^+, 144^-\}$	153
$\langle \Sigma^+\Sigma^-\overline{\Sigma^0_{X_q}\Lambda_{X_q}}\rangle$ $(q = u, d)$	2	$\{36^-, 36^+\}$	72
$\langle \Sigma^+\Sigma^-\overline{\Sigma^0_{X_q}\Lambda_{X_{q'}}}\rangle$ $((q,q')=(d,u),(u,d))$	2	$\{9^+, 144^-\}$	153
$\langle \Sigma^+\Sigma^-\overline{\Sigma^0_{X_q}\Lambda_{X_s}}\rangle$ $(q = u, d)$	2	$\{144^-, 36^+\}$	180
$\langle \Sigma^0\Sigma^0\overline{\Lambda_{X_q}\Lambda_{X_{q'}}}\rangle$ $(q = q')$	8	$\{1^+, 9^-, 144^-, 144^+, 144^-, 144^+, 9^+, 1^-\}$	596
$\langle \Sigma^0\Sigma^0\overline{\Lambda_{X_q}\Lambda_{X_{q'}}}\rangle$ $(q \neq q')$	8	$\{1^+, 36^-, 144^-, 36^+, 36^-, 144^+, 36^+, 1^-\}$	434
$\langle \Sigma^0\Sigma^0\overline{p\Xi^-}\rangle$	8	$\{36^+, 144^-, 9^-, 36^+, 36^-, 9^+, 144^+, 36^-\}$	450
$\langle \Sigma^0\Sigma^0\overline{n\Xi^0}\rangle$	8	$\{36^+, 36^-, 9^-, 144^+, 144^-, 9^+, 36^+, 36^-\}$	450
$\langle \Sigma^0\Sigma^0\overline{\Sigma^+\Sigma^-}\rangle$	8	$\{36^-, 144^+, 36^+, 9^-, 9^+, 36^-, 144^-, 36^+\}$	450
$\langle \Sigma^0\Sigma^0\overline{\Sigma^0_{X_q}\Sigma^0_{X_{q'}}}\rangle$ $(q = q')$	8	$\{1^+, 9^-, 144^-, 144^+, 144^-, 144^+, 9^+, 1^-\}$	596
$\langle \Sigma^0\Sigma^0\overline{\Sigma^0_{X_q}\Sigma^0_{X_{q'}}}\rangle$ $(q \neq q')$	8	$\{1^-, 36^+, 144^+, 36^-, 36^+, 144^-, 36^-, 1^+\}$	434
$\langle \Sigma^0\Lambda\overline{p\Xi^-}\rangle$	8	$\{36^+, 144^-, 9^-, 36^+, 36^-, 9^+, 144^+, 36^-\}$	450
$\langle \Sigma^0\Lambda\overline{n\Xi^0}\rangle$	8	$\{36^+, 36^-, 9^-, 144^+, 144^-, 9^+, 36^+, 36^-\}$	450
$\langle \Sigma^0\Lambda\overline{\Sigma^+\Sigma^-}\rangle$	8	$\{36^-, 144^+, 36^+, 9^-, 9^+, 36^-, 144^-, 36^+\}$	450
$\langle \Sigma^0\Lambda\overline{\Sigma^0_{X_q}\Lambda_{X_{q'}}}\rangle$ $(q = q')$	8	$\{1^+, 9^-, 144^-, 144^+, 144^-, 144^+, 9^+, 1^-\}$	596
$\langle \Sigma^0\Lambda\overline{\Sigma^0_{X_q}\Lambda_{X_{q'}}}\rangle$ $(q \neq q')$	8	$\{1^-, 36^+, 144^+, 36^-, 36^+, 144^-, 36^-, 1^+\}$	434

28

Table 4: Same as Table 1 but for the channels with the strangeness $S = -3$ and -4.

channel	# of diagrams	$\{(\text{\# of iterations})^{\text{sign}}\}$	# of total iterations
$\langle \Xi^-\Lambda\overline{\Xi^-\Lambda}_{X_{u,s}}\rangle$	6	$\{1^+, 36^-, 144^+, 144^-, 36^+, 9^-\}$	370
$\langle \Xi^-\Lambda\overline{\Xi^-\Lambda}_{X_d}\rangle$	6	$\{1^+, 36^-, 144^+, 36^-, 144^+, 36^-\}$	397
$\langle \Xi^-\Lambda\overline{\Sigma^-\Xi^0}\rangle$	6	$\{36^-, 9^+, 144^-, 144^+, 36^-, 36^+\}$	405
$\langle \Xi^-\Lambda\overline{\Sigma^0_{X_u}\Xi^-}\rangle$	6	$\{36^+, 9^-, 144^+, 36^-, 144^+, 1^-\}$	370
$\langle \Xi^-\Lambda\overline{\Sigma^0_{X_d}\Xi^-}\rangle$	6	$\{144^-, 36^+, 36^-, 36^+, 144^-, 1^+\}$	397
$\langle \Sigma^-\Xi^0\overline{\Xi^-\Lambda}_{X_u}\rangle$	3	$\{36^-, 144^+, 36^-\}$	216
$\langle \Sigma^-\Xi^0\overline{\Xi^-\Lambda}_{X_d}\rangle$	3	$\{9^-, 36^+, 144^-\}$	189
$\langle \Sigma^-\Xi^0\overline{\Xi^-\Lambda}_{X_s}\rangle$	3	$\{36^-, 144^+, 144^-\}$	324
$\langle \Sigma^-\Xi^0\overline{\Sigma^-\Xi^0}\rangle$	3	$\{1^+, 144^-, 36^+\}$	181
$\langle \Sigma^-\Xi^0\overline{\Sigma^0_{X_u}\Xi^-}\rangle$	3	$\{36^-, 36^+, 144^-\}$	216
$\langle \Sigma^-\Xi^0\overline{\Sigma^0_{X_d}\Xi^-}\rangle$	3	$\{144^+, 9^-, 36^+\}$	189
$\langle \Sigma^0\Xi^-\overline{\Xi^-\Lambda}_{X_{u,s}}\rangle$	6	$\{9^+, 36^-, 144^+, 144^-, 36^+, 1^-\}$	370
$\langle \Sigma^0\Xi^-\overline{\Xi^-\Lambda}_{X_d}\rangle$	6	$\{36^+, 144^-, 36^+, 144^-, 36^+, 1^-\}$	397
$\langle \Sigma^0\Xi^-\overline{\Sigma^-\Xi^0}\rangle$	6	$\{36^-, 36^+, 144^-, 144^+, 9^-, 36^+\}$	405
$\langle \Sigma^0\Xi^-\overline{\Sigma^0_{X_u}\Xi^-}\rangle$	6	$\{1^+, 144^-, 36^+, 144^-, 9^+, 36^-\}$	370
$\langle \Sigma^0\Xi^-\overline{\Sigma^0_{X_d}\Xi^-}\rangle$	6	$\{1^-, 144^+, 36^-, 36^+, 36^-, 144^+\}$	397
$\langle \Xi^-\Xi^0\overline{\Xi^-\Xi^0}\rangle$	6	$\{1^+, 36^-, 9^+, 144^+, 36^-, 144^+\}$	370

Table 5: Measured elapsed time for various hybrid parallel computation of the 52 four-point correlation functions $\sum_{\vec{X}} \left\langle B_{1,\alpha}(\vec{X}+\vec{r},t)B_{2,\beta}(\vec{X},t)\overline{\mathcal{J}_{B_{3,\alpha'}B_{4,\beta'}}(0)} \right\rangle$, $(t = 0, \cdots, T-1)$, by using the 32 node of BlueGene/Q on a $L^3 \times T = 16^3 \times 32$ lattice, changing the number of MPI processes (tasks_per_node) and the number of threads (OMP_NUM_THREADS). A computational job consists of two steps; to calculate all of the single baryon blocks $[B_\alpha^{(I)}]$ together with its FFT (step-1), and to calculate the 52 four-point correlation functions by performing the summations of indices of colour and spinor together with its inverse FFT (step-2).

[tasks_per_node] ×[OMP_NUM_THREADS]	64×1	32×2	16×4	8×4	4×8	2×16	1×32
Step-1	00:14	00:16	00:09	00:09	00:07	00:06	00:06
Step-2	00:10	00:11	00:12	00:12	00:12	00:13	00:14

Table 6: Comparisons of numerical results between this work and the other [29] are shown for only 16 lines of the four-point correlation function $\sum_{\vec{X}} \left\langle p_\alpha(\vec{X}+\vec{r},t)\Lambda_\beta(\vec{X},t)\overline{\mathcal{J}_{p_{\alpha'}\Lambda_{\beta'}}(t_0)} \right\rangle$ at $t - t_0 = 10$. "Diff" is the difference between "This work" and "Other".

$\tilde{\alpha}$	$\tilde{\beta}$	$\tilde{\alpha}'$	$\tilde{\beta}'$	x	y	z	This work	Other [29]	Diff
0	1	0	1	0	0	0	-3.075847140449e-21	-3.075847140449e-21	3.4e-36
0	1	0	1	1	0	0	-8.786230541230e-21	-8.786230541230e-21	-3.0e-35
0	1	0	1	2	0	0	-1.138496114849e-20	-1.138496114849e-20	-3.8e-35
0	1	0	1	3	0	0	-8.109792412599e-21	-8.109792412599e-21	-2.4e-35
0	1	0	1	4	0	0	-1.086965914839e-20	-1.086965914839e-20	-2.9e-35
0	1	0	1	5	0	0	-9.926801964792e-21	-9.926801964792e-21	-6.0e-36
0	1	0	1	6	0	0	-6.647331180826e-21	-6.647331180826e-21	2.0e-35
0	1	0	1	7	0	0	-1.640062750340e-21	-1.640062750340e-21	5.0e-35
0	1	0	1	8	0	0	-2.553910496200e-21	-2.553910496200e-21	7.0e-35
0	1	0	1	9	0	0	-1.250692150908e-22	-1.250692150907e-22	7.3e-35
0	1	0	1	10	0	0	4.866793580424e-21	4.866793580424e-21	9.4e-35
0	1	0	1	11	0	0	1.379986127982e-20	1.379986127982e-20	1.2e-34
0	1	0	1	12	0	0	1.680166855166e-20	1.680166855166e-20	9.9e-35
0	1	0	1	13	0	0	1.176203581648e-20	1.176203581648e-20	6.2e-35
0	1	0	1	14	0	0	2.994087733578e-21	2.994087733579e-21	3.1e-35
0	1	0	1	15	0	0	-9.904925605073e-22	-9.904925605073e-22	2.4e-35

Table A.7: The number of effective baryon block objects declared and the memory size of each baryon block object for a calculation of the 52 NBS wave functions given in Eqs. (34)−(38) for taking a normal approach or the improved (aggregative) approach described in Appendix A. The ratio of aggregative to normal is also presented. For the $2+1$ flavour lattice QCD calculation, a quantity of X_d can be replaced by the corresponding quantity from X_u. Thus no actual memory is required for the X_d for the improved algorithm.

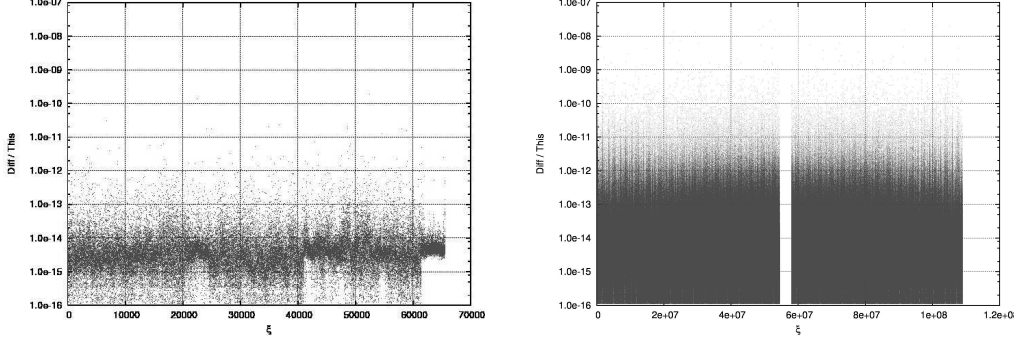|		p	Σ^+	Ξ^0	X_u	X_d	X_s
Number of baryon blocks	Normal	304	124	298	1784	1784	984
	Aggregative	28	18	19	36	0	32
	Ratio (%)	9.21	14.5	6.38	2.02	0	3.25
Memory size ($\times 16$ Bytes/site)	Normal	120144	46960	106104	554896	554896	305896
	Aggregative	10952	7208	7784	12128	0	10968
	Ratio (%)	9.12	15.3	7.34	2.19	0	3.59

Figure 2: (Left) The relative difference, $|\frac{\text{Diff}}{\text{This work}}|$, of the correlation function $\sum_{\vec{X}} \left\langle p_\alpha(\vec{X}+\vec{r},t)\Lambda_\beta(\vec{X},t)\overline{\mathcal{J}_{p_{\alpha'}\Lambda_{\beta'}}(t_0)} \right\rangle$ at $t-t_0 = 10$, between the effective block algorithm and the unified contraction algorithm as a function of one-dimensionally aligned data point $\xi = \tilde{\alpha}+2(\tilde{\beta}+2(\tilde{\alpha'}+2(\tilde{\beta'}+2(x+16(y+16(z))))))$. (Right) The relative difference of the correlators of entire 52 channels from NN to $\Xi\Xi$ given in Eqs. (34)−(38), over 31 time-slices, 16^3 points for spatial, and 2^4 points for the spin degrees of freedom, between the effective block algorithm and the unified contraction algorithm as a function of one-dimensionally aligned data point $\xi = \tilde{\alpha}+2(\tilde{\beta}+2(\tilde{\alpha'}+2(\tilde{\beta'}+2(x+16(y+16(z+16(c+52((t-t_0+T) \bmod T)))))))))$, where $c = 0,\cdots,51$ selects one of the 52 channels provided that the correlator has non-vanishing value.
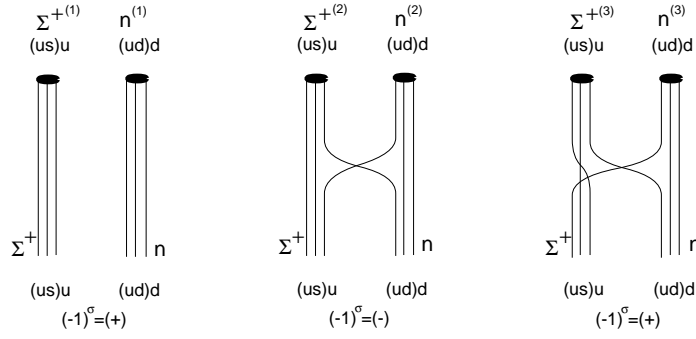

Figure A.3: Diagrammatic representation of the four-point correlation function $\langle\Sigma^+ n\overline{\Sigma^+ n}\rangle$. Three diagrams correspond to the three terms in Eq. (A.3). The parity of each permutation is also shown as $(-1)^\sigma$.

31